Scenario-based numerical modelling and the palaeo-historic record of tsunamis in Wallis and Futuna, Southwest Pacific

G. Lamarche, S. Popinet, B. Pelletier, J. Mountjoy, J. Goff, S. Delaux, J. Bind

Nat. Hazards Earth Syst. Sci., 15, 1763–1784, 2015
www.nat-hazards-earth-syst-sci.net/15/1763/2015/
doi:10.5194/nhess-15-1763-2015

Natural Hazards and Earth System Sciences
Open Access

Scenario-based numerical modelling and the palaeo-historic record of tsunamis in Wallis and Futuna, Southwest Pacific

G. Lamarche[1], S. Popinet[1,a], B. Pelletier[2], J. Mountjoy[1], J. Goff[3], S. Delaux[1,b], and J. Bind[4]

[1]National Institute of Water & Atmospheric (NIWA) Research, 301 Evans Bay Parade, Wellington 6021, New Zealand
[2]Institut de Recherche pour le Développement, BP A5, Nouméa, New Caledonia
[3]School of Biological, Earth and Environmental Sciences, UNSW Australia, Sydney 2052, Australia
[4]NIWA, 10 Kyle Street, Christchurch 8011, New Zealand
[a]now at: CNRS – Université Pierre et Marie Curie Paris 6, Institut Jean Le Rond d'Alembert, 75005 Paris, France
[b]now at: MetOcean Solutions Ltd. 5 Wainui Rd, Raglan 3225, New Zealand

Correspondence to: G. Lamarche (geoffroy.lamarche@niwa.co.nz)

Received: 20 November 2014 – Published in Nat. Hazards Earth Syst. Sci. Discuss.: 8 April 2015
Accepted: 16 July 2015 – Published: 11 August 2015

Abstract. We investigated the tsunami hazard in the remote French territory of Wallis and Futuna, Southwest Pacific, using the Gerris flow solver to produce numerical models of tsunami generation, propagation and inundation. Wallis consists of the inhabited volcanic island of Uvéa that is surrounded by a lagoon delimited by a barrier reef. Futuna and the island of Alofi form the Horn Archipelago located ca. 240 km east of Wallis. They are surrounded by a narrow fringing reef. Futuna and Alofi emerge from the North Fiji Transform Fault that marks the seismically active Pacific-Australia plate boundary. We generated 15 tsunami scenarios. For each, we calculated maximum wave elevation (MWE), inundation distance and expected time of arrival (ETA). The tsunami sources were local, regional and distant earthquake faults located along the Pacific Rim. In Wallis, the outer reef may experience 6.8 m-high MWE. Uvéa is protected by the barrier reef and the lagoon, but inundation depths of 2–3 m occur in several coastal areas. In Futuna, flow depths exceeding 2 m are modelled in several populated areas, and have been confirmed by a post-September 2009 South Pacific tsunami survey. The channel between the islands of Futuna and Alofi amplified the 2009 tsunami, which resulted in inundation distance of almost 100 m and MWE of 4.4 m. This first ever tsunami hazard modelling study of Wallis and Futuna compares well with palaeotsunamis recognised on both islands and observation of the impact of the 2009 South Pacific tsunami. The study provides evidence for the mitigating effect of barrier and fringing reefs from tsunamis.

1 Introduction

Awareness of the potential disastrous consequences of tsunamis for coastal regions has been exacerbated over the last 10 years with events in Sumatra (2004), Tonga-Samoa (2009) and Japan (2011), to name only three of the most significant (Løvholt et al., 2012; Sahal et al., 2010; Satake et al., 2013). These events have emphasised the deficiency in our understanding of tsunami processes and their impact on local communities and has sparked an increase in tsunami-related research. Yet the focus of the research has generally been on impacted coasts or in highly populated areas. Because of their remoteness and their low populations, many Pacific Island Countries and Territories (PICT), have been omitted from this research effort, even though the tsunami hazard is a reality for all islands in the Pacific (e.g., Dominey-Howes and Goff, 2013; Goff, 2011; Goff et al., 2010b; Hébert et al., 2001; Sahal et al., 2010; Schindelé et al., 2006).

Whether natural features such as reefs, lagoon or mangroves provide protection from tsunamis still remains a matter of debate (Baba et al., 2008; Gelfenbaum et al., 2011; Hébert et al., 2001; Roger et al., 2012). These authors have highlighted the importance of reef morphology and the immediate seaward slope on tsunami inundation, including focusing effects resulting from channels and embayments. In particular, Gelfenbaum et al. (2011) discuss the mitigating effects of barrier and fringing reefs on tsunami inundation, including their surface roughness and width, but there is no unequivocal correlation between reef morphologies and tsunami inundation hazard. This is critical for the numerous

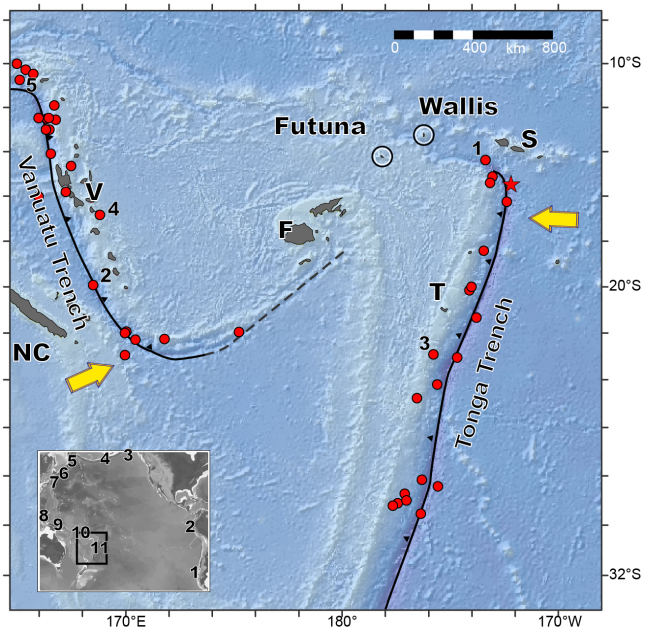

Figure 1. The Southwest Pacific region – star indicates location of the 29 September 2009 $M_W = 8.1$ South Pacific earthquake. Earthquakes $M > 8$ are indicated with red dots Source USGS (http://earthquake.usgs.gov/). Earthquakes mentioned in the text are labelled by year: (1): 26 June 1917 $M_W = 8$ Samoa; (2): 20 September 1920 $M_W = 7.8$ Loyalty Island; (3): 22 June 1977 $M_W = 8.1$ Tonga; (4): 26 November 1999 $M_W = 7.5$ Ambrym; (5): 6 February 2013 $M_W = 8.0$ Santa Cruz. NC: New Caledonia, V: Vanuatu, F: Fiji, S: Samoa, T: Tonga. Insert: the Pacific Basin. Number are the approximate location of tsunami sources as indicated in Table 2.

low-lying islands of the Pacific which have not been the recipient of many tsunami hazard studies such as in Tokelau (Orpin et al., 2015) or in the Marquesas (Hébert et al., 2001).

The French territory of Wallis and Futuna (W&F), in the Southwest Pacific (Fig. 1), is not protected from tsunamis as demonstrated by the events that have struck Futuna in the past – either in modern era as in 1993 (Louat et al., 1989b; Régnier, 1994) and 2009 (Lamarche et al., 2010), or in prehistoric times (Goff et al., 2011, 2010a).

This project follows on from a research initiative in Futuna (Lamarche et al., 2009) and Wallis (Mountjoy et al., 2011), which aimed to assess the tsunami hazard in both archipelagos. The project included palaeotsunami research from geological markers of rapid marine invasions, observations of the impact of the September 2009 South Pacific tsunami and numerical modelling of tsunami scenarios. Whereas some incidental observations and research on tsunamis has taken place in Futuna and Alofi (Capecchi, 1995; Louat et al., 1989b; Monzier et al., 1993), there has been no such studies on Wallis. Further work was undertaken for the territorial administration of W&F and presented in an unpublished report (Lamarche et al., 2013).

This paper documents the tsunami hazards in Wallis and in Futuna from the generation and interpretation of 15 numerical models for scenarios affecting both archipelagos. Here we focus exclusively on tsunamis generated by earthquakes originating from the Pacific Rim, the sources of which are identified and characterised using published data. Other sources such as volcanic eruptions, submarine or subaerial landslides or meteorite impacts are not considered. We use the Gerris flow solver (Popinet, 2003, 2011) to produce numerical models of tsunami generation, propagation and inundation. The models are validated by comparing with field observation of historical and palaeo-historical tsunami impacts on these islands. The resulting hazard, in terms of wave elevation and inundation distances on the coastal areas in W&F are discussed. Our results provide a means to discuss and compare the mitigating impact of barrier and fringing reefs on tsunamis along the inhabited coasts of W&F. This paper however does not discuss the likelihood of events, as it is essentially related to the probability of occurrence of earthquake generating tsunamis which is beyond the scope of this study. Nor does this paper discuss the risk resulting from tsunamis, although it provides valuable information toward developing such assessments of risk.

2 Settings

2.1 Tectonics of the Southwest Pacific

Earthquakes of magnitudes large enough to generate transoceanic tsunamis have occurred along the subduction trenches that delimit the rim of the Pacific Basin (Insert Fig. 1). Although the two most memorable events are the 1960 $M_W = 9.5$ Chile (the largest documented historical earthquake) and 2011 $M_W = 9.1$ Japan (the most recent catastrophic tsunami-generating event) earthquakes, a number of events with magnitude greater than 8 have occurred in the 20th and 21st centuries (Table 1).

In the Southwest Pacific region, intense tectonic activity originates from the Pacific-Australia convergent plate boundary and the broad area of deformation of the North Fiji Basin-Lau Basin that accommodates the transition between the opposite-facing and partly overlapping Tonga and Vanuatu subduction zones (Fig. 1). This tectonically complex region consists of intersecting and overlapping compressional tectonic features along subduction trenches, extensional rifts along back-arc basins and transform faults (Fig. 2 and Pelletier et al., 1998).

The rate of frontal subduction of 24 cm yr^{-1} that occurs at the northern end of the Tonga Trench is the fastest recorded globally (DeMets et al., 2010; Pelletier and Louat, 1989). Northward, the Tonga Trench turns sharply to the west and deformation is transferred to the 1500 km-long North Fiji Transform Fault Zone (NFTFZ), along which the strike-slip

Table 1. The ten largest offshore Pacific earthquakes since 1900 and Southwest Pacific earthquakes of $M_W = > 8.1$ since 1950, in decreasing magnitude. (Data from USGS, see http://earthquake.usgs.gov/earthquakes). The "Loc." column indicates the approximate location of the epicentres on Fig. 1.

Date	Latitude	Longitude	M_W	Loc	Comment
22/05/1960	38.29° S	73.05° W	9.5	1	Chile
28/03/1964	61.02° N	147.65° W	9.2	3	Prince William Sound, Alaska
4/11/1952	52.76° N	160.06° E	9	5	Kamchatka, Russia
11/03/2011	38.322° N	142.369° E	9	7	East coast, Honshu, Japan
31/01/1906	1° N	81.5° W	8.8	2	Colombia-Ecuador
27/02/2010	35.846° S	72.719° W	8.8	1	Maule, Chile
4/02/1965	51.21° N	178.5° W	8.7	4	Rat Islands, Alaska
9/03/1957	51.56° N	175.39° W	8.6	4	Andreanof Islands, Alaska
3/02/1923	54° N	161° E	8.5	5	Kamchatka
13/10/1963	44.9° N	149.6° E	8.5	6	Kuril Islands
19/08/1977	11.085° S	118.464° E	8.3	8	South of Sumbawa, Indonesia
17/02/1996	0.891° S	136.952° E	8.2	8	Irian Jaya region, Indonesia
10/01/1971	3.132° S	139.697° E	8.1	9	Papua, Indonesia
22/06/1977	22.878° S	175.9° W	8.1	11	Tonga region
1/04/2007	8.466° S	157.043° E	8.1	10	Solomon Islands
29/09/2009	15.489° S	172.095° W	8.1	11	Samoa Islands region
15/11/2006	46.607° N	153.230° E	8.3	6	Central Kuril
15/01/2007	46.272° N	154.455° E	8.1	6	Kuril–Kamchatka Trench

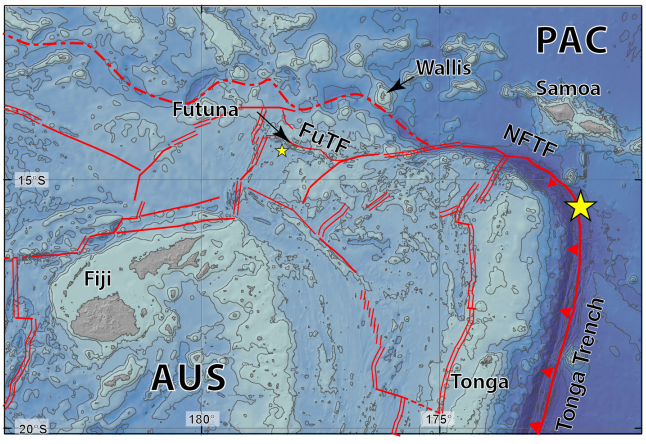

Figure 2. Seafloor morphology and main tectonics features of the northern Fiji Basin. Double red lines indicate active spreading centres; plain lines are fracture zones; dash lines are inactive structures, and teeth line indicates the subduction front of the Pacific-Australia (PAC-AUS) plate boundary. NFTF: North Fiji Transform Fault Zone; FuTF: Futuna Transform Fault. Large yellow star is epicentre of the 29 September 2009 South Pacific Earthquake; small yellow star is epicentre of March 1993 Futuna Earthquake (Monzier et al., 1993; Régnier, 1994).

rate decreases to 8.5 cm yr^{-1} at the longitude of Futuna (Pelletier et al., 2001; Pelletier et al., 2000a).

Twenty shallow earthquakes of magnitude larger than or equal to $M_W = 7.5$ have occurred in the Tonga-Kermadec region since 1900 (http://earthquake.usgs.gov/earthquakes, Fig. 1; Engdahl and Villasenor, 2002). Five earthquakes are larger than or equal to $M_W = 8$, and include the 29 September 2009 $M_W = 8.1$ and 26 June 1917 $M_W = 8$ earthquakes with epicentres located along the northern Tonga Trench. Although the NFTFZ is a predominantly strike-slip structure, several thrust earthquakes have occurred along its length thanks to restraining bends, as in the $M_W = 6.3$ 1993 Futuna earthquake (Régnier, 1994).

To the west of the North Fiji Basin, the Pacific-Australia plate boundary runs along the Vanuatu Trench (also named New Hebrides Trench) immediately west of the Vanuatu archipelago (Fig. 1). Frontal subduction occurs along the Vanuatu Trench, which separates into northern, central and southern segments at 13° S and ca. 17° S. Rates of subduction are 17 cm yr^{-1} in the north and ca. 12 cm yr^{-1} in the south (Louat et al., 1989a; Pelletier and Louat, 1989).

East of the central Vanuatu archipelago, compressional tectonics at a rate of 5–6 cm yr^{-1} along the Vanuatu back-arc originates from the collision of the d'Entrecasteaux ridge with the central part of the Vanuatu Arc to the west of the archipelago (Pelletier et al., 1998; Regnier et al., 2003).

Seismicity is also prevalent in the Vanuatu region, with 21 shallow earthquakes of magnitude larger than or equal to $M_W = 7.5$ recorded since 1900. Examples include the 20 September 1920 $M_W = 7.8$ Loyalty Island event along the southern part of the trench, and the 6 February 2013 $M_W = 8.0$ Santa Cruz earthquake along the northern part. Of particular interest to this study is the 26 November 1999 $M_W = 7.5$ Ambrym earthquake which occurred in the southern part of the central Vanuatu back arc thrust and generated

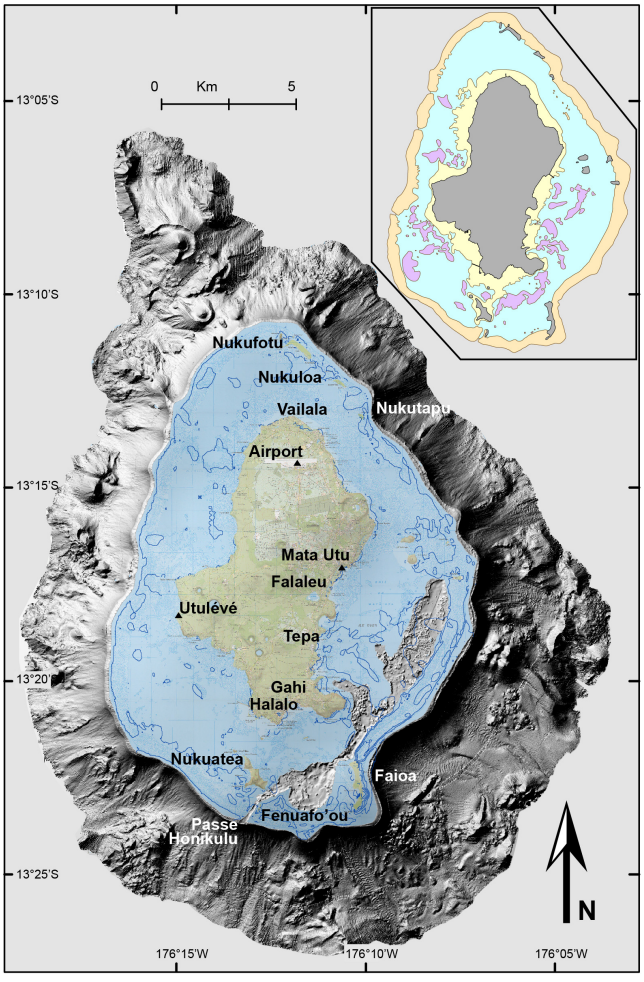

Figure 3. Wallis archipelago. Land and lagoon coloured map from IGN (2007b); the shaded seafloor topography of the seaward reef wall is from the WALFUT survey (Pelletier et al., 2011). Insert shows land in grey and reef types as barrier reef (orange), fringing reef (yellow) and patch reef (pink) from the Reef Base database (http://www.reefbase.org).

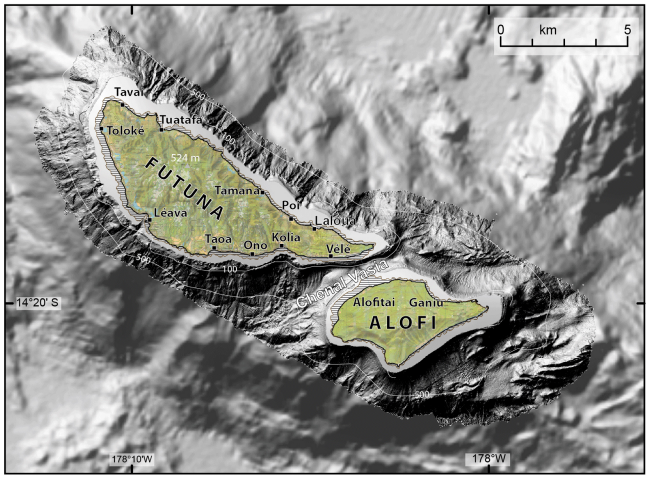

Figure 4. The Horn Archipelago, Futuna and Alofi islands. Land coloured map from IGN (2007a). The fringing reef (dark grey) is from the Reef Base database. The shaded high-resolution seafloor topography of the seaward reef wall is from the WALFUT survey (Pelletier et al., 2011). The low resolution bathymetry outside the reef wall is from the ALAUFI Cruise (Pelletier et al., 2001). The white contours offshore are 100 and 500 m water depth.

a large tsunami in Vanuatu (Ioualalen et al., 2006; Pelletier et al., 2000b; Regnier et al., 2003).

2.2 Wallis and Futuna

The French territory of W&F, in the SW Pacific, consists of the Wallis and Horn Archipelagos approximately 240 km apart (Fig. 1). Despite their relative proximity, the geodynamic settings of these two archipelagos differ significantly.

Wallis Archipelago (176°10′ W, 13°18′ S) is located approximately 480 km west of Samoa. It consists of the ca. 70 km^2 island of Uvéa which rises up to 115 m above mean sea level (a.s.l.) and is surrounded by a lagoon delimited by a barrier reef (Fig. 3). The lagoon is deepest to the SE, off the town of Mata'Utu, and reaches depths of 35 m with average depth of ca. 20 m. A number of small islands (approximately 17 "ilots") rest on top of both barrier and fringing reefs to the north, east and south of Uvéa. The islands on the barrier reef are surrounded by water at high tide and connect with each other through the reef at low tide. The west side of Wallis is dominated by a large fringing reef that connects with the barrier reef (insert Fig. 3). Only four narrow channels (passes) cut through the barrier reef to the south and west. The largest one to the south is ca. 160 m wide and 32 m deep. Uvéa has a population of ca. 9200 (July 2008 census). An unknown proportion of the population lives on the coastal fringe where much of the agriculture also takes place. A 350 m-long container wharf extends into the lagoon at Mata Utu, and a 550 m-long oil tanker wharf is located in Halalo, on the SW corner of the island, both representing important economic infrastructures on the island.

The Horn Archipelago (178°06′ W, 14°18′ S) consists of the islands of Futuna (83 km^2) and Alofi (32 km^2), located approximately 560 km NE of Viti Levu, Fiji (Fig. 4). Futuna has a 50 to 400 m-wide coastal strip that abuts landward coastal cliffs rising to over 500 m a.s.l. Alofi rises to over 400 m a.s.l. Both islands are surrounded by a narrow fringing reef, and there is no lagoon around Futuna or Alofi. At its widest, the fringing reef is 400–500 m on the SW coast of Futuna and the west coast of Alofi, and is generally less than 150 m wide elsewhere. The NE coast of Futuna has sandy beaches, whereas in the SW the coast is directly connected to the reef. Alofi's coast consists of sand beaches separated by small headlands. Futuna has a population of around 4250 (July 2008 census) and Alofi is uninhabited.

Because of the small size of these islands, the coastal fringe, i.e. within ~ 100 m of the coast and within ~ 5 m a.s.l., is scattered with domestic dwellings and most public infrastructure. Importantly for risk assessments, crops and most livestock are farmed on the coastal fringe. The population lives along the coastal road of Futuna within < 200 m of the coastline, in most cases no higher than 10 m a.s.l. – except for the settlement of Ono rising to ca. 50 m a.s.l., and the hospital, at Taoa, at 30 m a.s.l. The only commercial runway is located on reclaimed land at the SE tip of Futuna at an elevation of about 5 m a.s.l.

Futuna and Alofi islands emerge from the Futuna-Alofi volcanic ridge (Fig. 2). The ridge formed over a compressional relay along the NFTFZ which resulted in a series of thrust faults as close as 10 km SW of Futuna. This active tectonic setting results in the uplift of both islands (Pelletier et al., 2001). Variations in the rates of uplift suggest that active faults run between Futuna and Alofi (Pelletier et al., 2000a).

3 Tsunami hazard in Wallis and Futuna

3.1 Historical tsunamis

While there is some historical information on tsunamis for Futuna and Alofi (Table 2), we found no record concerning tsunamis having reached Wallis.

The most recent tsunami to have struck Futuna occurred on 30 September 2009 (local time). It was generated by the 29 September 2009 South Pacific $M_W = 8.1$ earthquake that occurred on the northernmost tip of the Tonga Trench (Beavan et al., 2010; Lay et al., 2010) (Fig. 1). The tsunami had a severe impact on Samoa, American Samoa and Tonga with a maximum run-up of 17.9 m, a maximum inland inundation distance of 500 m and over 190 casualties (Dominey-Howes et al., 2009; NGDC, 2014). Prior to this event, a tsunami occurred on 26 June 1917 which was generated by an earthquake from the same section of the Tonga Trench. Tsunami run-up in this case was about 12 m on Samoa (Okal et al., 2010).

The 2009 South Pacific tsunami reached Futuna and Alofi between 7:00 and 7:20 am on 30 September and its impact was assessed during a 10 day post-event survey soon after (Lamarche et al., 2010). An estimated maximum run-up of 4.5 m, inundation distance of 85 m and Maximum Wave Elevation (MWE) of 3 m were recorded on the eastern beach of Alofi. On Futuna, maximum run-up values of 4.4 and 4.3 m were inferred on the eastern side and the NW tip of the island, with respective inundation distances of 95 and 72 m. A MWE of 2 m was inferred on the NE side of Futuna in the village of Tavai (Fig. 4). Overall, the tsunami impact was more severe on the north of Futuna, with run-ups ranging from 1.6 to 4.3 m. Only small run-ups and inundation distances were observed along the south and west coasts, with 1.0 m and 10 m respectively at Léava.

Three areas of potentially high tsunami impact were determined during the post-tsunami survey: (1) Chenal Vasia between Futuna and Alofi. At Vélé, an MWE of 4.5 m and inundation distance of 95 m were estimated; (2) NW Futuna with MWE of 3.6 m and inundation distance of 40 m; and (3) north-east coast of Futuna, with a maximum inundation distance at Laloua of 60 m but with an undetermined MWE.

The only other historical event reported was a small tsunami along Futuna's south coast observed immediately after, and therefore assumed to be associated with the 12 March 1993 $M_W = 6.3$ earthquake (Capecchi, 1995; Monzier et al., 1993). In 1840, strong ground shaking and intense building damage described by the missionary station of St Pierre Chanel has also been associated with an earthquake (Régnier, 1994), but no tsunami was reported at the time. Local earthquakes, potentially triggering landslides and tsunamis are regularly felt in Futuna (Louat et al., 1989b).

3.2 Palaeotsunamis

Two events prior to European settlement have been inferred from palaeotsunami research and local oral traditions (Table 2).

Palaeotsunami research is conducted through the investigation of a suite of proxy data (Chagué-Goff and Goff, 1999; Goff et al., 2001, 2012a). In Futuna, more than 200 soil samples were taken from 10 trenches specifically dug in the search for the geological evidence of past events (Goff et al., 2010a; Lamarche et al., 2009). Most trenches show one or two soil layers covered by marine sand and corals debris, indicating potentially major marine inundations. The most recent event was time-correlative across several trenches and was also associated with an oral tradition recalling the village of Tavai, NE Futuna, being destroyed by a large wave (Di Piazza and Frimigacci, 1991; Frimigacci et al., 1995). Well constrained radiocarbon dates bracketing this palaeotsunami deposit provided an age of around 470 BP (years Before Present, i.e. ca. AD 1480) for this event (Goff et al., 2010a). An earlier event was dated using both radiocarbon and archaeological artefacts between 1860 and 2000 BP.

On the west coast of Wallis, at the abandoned settlement of Utulévé, where the fringing reef connects with the barrier reef (Fig. 3), trenching for palaeotsunami studies revealed marine sediments overlying a prehistoric occupation site represented by a pebble/cobble layer (unpublished data). The occupation site most likely records a period of human occupation that commenced with Polynesian arrival around 2750–2900 BP (Burley et al., 2011), followed later by the first (ca. AD 1000–1100) and second (ca. AD 1400) Tongan colonisations (Aswani and Graves, 1998; Frimigacci, 2000). On the east coast of Uvéa there is abundant evidence for storm/cyclone inundation, including overwash deposits and large boulders deposited on the reef crest (Mountjoy et al., 2011), but there is no clear evidence of tsunami-lain deposits. Unpublished data suggest that as opposed to sites on Futuna,

Table 2. Historical and palaeo-historical tsunami in Futuna

Date	Source/origin	Reference.
30 Sep 2009	Tonga Trench Earthquake	Lamarche et al. (2010, 2009)
12 March 1993	Futuna Ridge Earthquake	Monzier et al. (1993)
∼ 470 years BP (∼ 1450)	Unknown	Goff et al. (2011, 2009)
1860–2000 BP	Unknown	Goff et al. (2011, 2009)

Table 3. Characterising parameters of tsunami generated by the numerical modelling.

Parameter	Acronym	Definition
Maximum Wave Elevation	MWE	The maximum elevation above sea level reached within the model grid area relevant to that location.
Maximum Inundation Depth	MID	The maximum water height above ground floor resulting from the tsunami within the model grid.
Inundation distance		The shortest distance that the tsunami travels inland. Measured linearly from the shoreline.
Estimated Arrival Times	ETA	The time of arrival of the first wave (whether retreat or advance) at the coast. We include first arrival time corresponding to the onset of the inundation and last arrival time when sea has returned to a near normal state.

there is only one palaeo-tsunami event at Utulévé. Radiocarbon dates on charcoal and marine shell indicate that this event is most likely contemporaneous with the younger Futuna event around the 15th century.

The overall scenario for W&F fits with the archaeological record of human occupation and settlement pattern changes over the past 2000 years or more. There is published evidence for a significant region-wide palaeotsunami generated from the Tonga Trench around 2000 BP with effects noted throughout the Southwest Pacific (Goff et al., 2011, 2012b). It is most probable that both W&F would have been affected by such an event, although notable geological evidence has only been found on Futuna.

Evidence for a mid-15th century palaeotsunami is far more convincing in both Wallis and Futuna, and there is a considerable data set of supporting archaeological material. While people living on Futuna (and Alofi) consistently managed to repel the aggressive Tongan maritime expansion, those on Uvéa were successfully occupied twice, firstly around AD 1000 and secondly in the early 15th century (Aswani and Graves, 1998; Frimigacci, 2000). Goff et al. (2012b) surmise that it was followed by a large, region-wide tsunami that led to the widespread destruction of coastal settlements, an increase in warfare, the rise of chiefdoms and a significant resource crisis throughout the SW Pacific. More specifically, this could be linked to a movement of coastal settlements inland and uphill in both Wallis and Futuna, and the construction of forts on Uvéa (Frimigacci, 2000; Goff et al., 2012a; Williams, 2014).

4 Methods and data

4.1 Tsunamis numerical modelling

In this paper we only consider tsunamis generated by seafloor displacement associated with fault-rupturing earthquakes. Tsunami excitation grows proportionally to the vertical displacement at the seafloor generated during the event. Seafloor displacement is related to the moment magnitude (M_W) of the generating earthquake (e.g. Kanamori, 1972; Okal, 1988) and from the fault dip. M_W can be derived from the fault physical parameters (length, width, depth, dip) using empirical relationships (Hanks and Kanamori, 1979; Wells and Coppersmith, 1994). However, the relationship between earthquake magnitude and seafloor vertical displacement is complex (e.g., Okada, 1985), and results in uncertainties that have not been formally quantified in this study.

Tsunami ocean pathways and amplitude at the receiving shore are directly affected by focusing and defocusing effects due to bathymetric variations. The tsunami inundation height (MWE and run-up) and penetration inland (inundation distance) depend on coastal bathymetry, topography above the shoreline and human modification. Hence, physical parameters of the rupturing fault, ocean floor topography (bathymetry) and land topography are critically important for generating meaningful numerical tsunami modelling.

Here, we use the Gerris hydrodynamic software (see http://gfs.sourceforge.net, Popinet, 2003, 2011) for modelling tsunami initiation, propagation and inundation. The code was run from a standard single-processor desktop computer. The

initial wave elevation is obtained from a source model derived using seismic data. The simulation domain covers a significant part of the NW Pacific. Gerris uses adaptive mesh refinement whereby the spatial resolution is adapted dynamically from a maximum of 250 m in flooded areas and 250 km for areas at rest, and where wave fronts are tracked at a resolution of 1.8 km in deep water. This leads to orders-of-magnitude gains in computational efficiency compared to non-adaptive methods. The time required to process any one scenario was of the same order of magnitude as the real time of the event propagation, i.e. 1 h of processing time is equal to approximately 1 h of real time.

We used two sets of spatial resolution. One set was used for far-field scenarios, with a Pacific-wide maximum deep-water resolution of 1.6 km and a maximum resolution of 50 m close to W&F. A second set for near-field scenarios, used a maximum deep-water resolution of 250 m over no more than 4000×4000 km and a maximum resolution of 15 m close to the coast. Initial runs were typically performed using a $2\times$ coarser spatial resolution, which gave an indication of the sensitivity of the results to spatial variability. An additional 10 m resolution scenario was also run for the Futuna source.

In this paper we retained the four following characterising parameters of tsunami generated by the numerical modelling (Table 3): The modelled Maximum Wave Elevation (MWE); the modelled Maximum Inundation Depth (MID); the modelled inundation distance (also called run-out in the literature); and the Estimated Arrival Times (ETA) at the coast. The MWE at the maximum inundation distance equate therefore to the run-up used in many publications.

Wave heights, arrival times and travel pathways generated by Gerris tsunami models have been validated against laboratory benchmarks, sea level records during recent tsunami, and palaeotsunami data, including long-distance wave propagation and fine-scale flooding occurring during the 11 March 2011 Japan tsunami (Popinet, 2012). Accurate long-distance wave prediction has also been demonstrated through comparison with time series from DART (Deep-ocean Assessment and Reporting of Tsunamis) buoys and GLOSS (Global Sea Level Observing System) tide gauges records. Gerris has also accurately predicted fine-scale flooding compared with both satellite and survey data.

4.2 Land topography and lagoon bathymetry

While regional seafloor topography is acceptable in deep oceanic environments, the best possible accuracy is required in the coastal zone for numerical modelling of tsunami propagation. For this study, particular attention was devoted to generating integrated bathymetry – topography Digital Terrain Models (DTM) for Wallis and for Futuna-Alofi. The onshore DTMs for Wallis combines a variety of existing topographic (IGN, 2007a, b) and satellite derived data, with data collected using real time kinematic GPS and processed for this project (see Supplement).

In Futuna and Alofi, we digitised the 0, 5 and 10 m contour lines from the 1 : 25 000 topographic maps (IGN, 2007a) to generate the onshore DTM.

Seaward of the coast of Wallis and Futuna, we used the bathymetry of the Pacific Basin from the GEBCO data set.

In the vicinity of the islands, we used the SHOM bathymetric charts (SHOM, 2008, 2010), and the multibeam bathymetry data sets acquired during the ALAUFI survey, March 2001, (Pelletier et al., 2001, 2000a) around Futuna and Alofi and the WALFUT survey, June 2011 (Pelletier et al., 2011) around both archipelagos.

Bathymetric data in the Wallis lagoon are sparse, with depth data only available in the south and SE (Pelletier et al., 2011; SHOM, 2008). For the shallow (< 10 m) uncharted parts of the lagoon in the SW, NW and NE, we correlated the 4 spectral bands (red, green, blue and near-infrared) of the Quickbird satellite images with bathymetric contour lines in the mapped area (see Supplement for details). For depths greater than 10 m, we used information generated for marine habitat mapping from Andréfouët and Diberg (2006).

The seaward border of the reef in Futuna was digitised from Google Earth extracts and IGN topo maps.

In a final step, land-based and offshore DTMs were merged into two distinct sets for Wallis and for Futuna-Alofi.

5 Parameterisation of earthquake fault-sources

Since many tsunamis originating from NE Asia, NW America and South America have reached the coasts of New Zealand (Goff et al., 2010b; Power et al., 2007), the Cook Islands (Goff, 2011) and Hawaii (Chagué-Goff et al., 2012), we assume that earthquakes capable of generating tsunamis large enough to reach W&F occur all around the Pacific Rim. Here we discriminate between trans-Pacific (or tele-), regional and local earthquake sources, as it has relevance for characterising the source of tsunamis.

We consider that to be capable of generating a tsunami large enough to reach Wallis or Futuna, ocean-wide or regional earthquakes would typically have to be of magnitude greater than $M_W = 8.0$. Although somewhat arbitrary, this value is substantiated by recent and historical events (Kanamori, 1972; Satake and Tanioka, 1999; Sugawara et al., 2014). Indeed, local tsunamigenic earthquakes, affecting land areas within less than ca. 50 km of the source, need be of lesser magnitudes, and no lower magnitude is assumed for these events. In this study, this is only relevant to Futuna and Alofi.

The location and physical parameters (length, width, depth, dip) of the earthquake fault-sources required to generate the tsunamis were derived from information obtained in the international literature, and interpretation of multibeam bathymetry data acquired during the March 2000 ALAUFI (Pelletier et al., 2001, 2000a) and June 2011 WALFUT (Pelletier et al., 2011) oceanographic voyages. In all cases we

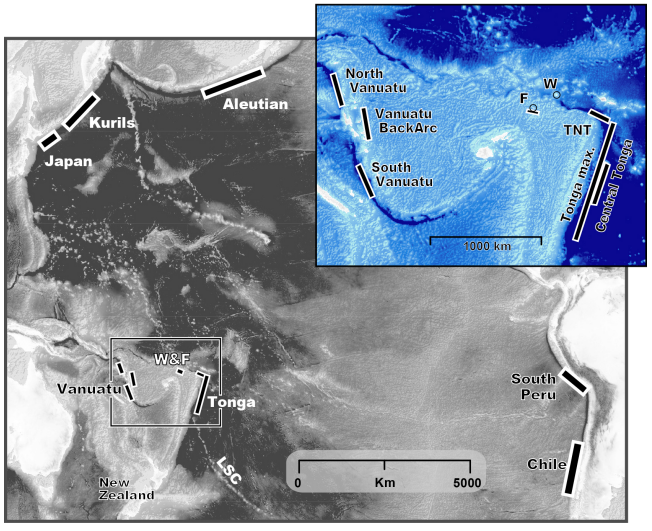

Figure 5. Earthquakes sources (black lines) used in this study tsunami models. Pacific-wide (grey map) and South Pacific (blue map). The lengths and orientations are that used in the models (see Table 4) LSC: Louisville Seamount Chain. Insert: enlargement over the Fiji Basin. W: Wallis; F: Futuna; TNT: Tip North Tonga source.

purposefully selected parameters that generated the largest plausible earthquake in the region using available data as a first order guide. In most cases these earthquakes have not happened in historical time, but are worst-case scenarios.

In this study we derive earthquake moment magnitudes from empirical correlations with fault rupture lengths and widths. The method was developed from global studies of historic earthquakes ruptures (Hanks and Kanamori, 1979; Okal et al., 2006; Wells and Coppersmith, 1994). We use the Hanks and Kanamori (1979) empirical regression:

$$M_{\mathrm{W}} = 2/3 \times \log(\mathrm{Mo}) - 10.7, \quad (1)$$

where the seismic moment (Mo) is calculated from

$$\mathrm{Mo} = \mu \mathrm{LWD}, \quad (2)$$

where μ is the rigidity modulus of the Earth's crust (3×10^{11} dyne cm^{-2}), L and W are fault length and width determined from bathymetry maps and literature review, and D is the single event displacement provided in the literature. No uncertainties were assigned to these dimensions as we consider them as maximum values.

5.1 Trans-pacific sources

All tele-earthquake sources are located along the Pacific Rim (Fig. 5) in the circum-Pacific deep subduction trenches of Japan, the Kurils, Aleutian, Cascadia, Peru and Chile, where earthquake magnitudes greater than $M_{\mathrm{W}} = 8.5$ have been recorded (Table 1). All earthquake fault parameters are overestimates of data from historical earthquakes retrieved from

Table 4. Summary of models' input parameters and results.

N	Scenario Name	Based on[1]	M_{W}^2	L[3] (km)	W[4] (km)	Slip[5] (m)	Dip (°)	Strike (°)	MWE[6] Wallis (m)	MWE[6] Futuna (m)	MID[7] Wallis (m)	MID[7] Futuna (m)	Arrival[8] Wallis	Arrival[8] Futuna
Tele tsunami sources (all rakes 90°)														
1	Japan	11 Mar 2011	9.0	700	50[9]	12.5	12	195	1.0	0.5	0.6	0.3	9 h05'–18 h50'	9 h20'–11 h20'
2	Kuril	worst case	9.28	1000	200	17	30	220	3.9	4.5	3.1	3.5	8 h35'–> 12 h	8 h50'–> 12 h
3	Aleutian Arc	9 Mar 1957	8.6	850	150	10	15	70	0.9	0.1	0.9	0	8 h50'–13 h40'	N/D[10]
4	Cascadia	worst case	9.1	1050	70	17.5	15	350	0.4	0	0.2	0	11 h40'–23 h40'	N/D[10]
5	Peru	13 Aug 1868	9.0	900	150	15	20	305	2.2	3.2	1.5	1.5	15 h–17 h30'	15 h30'–15 h40'
6	Chile	22 May 1960	9.29	920	120	32	12	10	0.7	0.5	0.4	0.1	13 h30'–22 h25'	14 h–15 h15'
Regional sources (all rakes 90°)														
7	Tonga 2009	29 Sep 2009	8.1	200[11]	50[11]	5–9.5[11]	57	342.5	2.7	8.7	2.2	8	0 h30'–2 h45'	1 h20'–6 h45'
8	Tonga	worst case	9.06	1000	80	20	30	195	6.8	11.1	5.6	9.8	0 h20'–3 h55'	0 h45'–3 h45'
9	Tonga + 1 m	worst case	9.06	1000	80	20	30	195	6.9	13.4	6.5	11.7	0 h25'–> 7 h	0 h45'–> 7 h
10	Central Tonga	worst case	8.57	600	50	10	30	200	1.7	1.2	1.3	1.1	1 h15'–3 h	1 h25'–5 h45'
11	North Tonga	worst case	8.16	300	40	6	60	100	3.0	1.7	2.7	1.4	0 h10'–1 h50'	1 h–1 h45'
12	North Vanuatu	worst case	8.39	400	40	10	30	350	0.5	1.1	0.2	1.0	3 h15'–3 h40'	2 h55'–3 h10'
13	South Vanuatu	worst case	8.24	300	40	8	30	335	0.4	0.9	0.4	0.3	3 h10'–7 h30'	2 h45'–2 h55'
14	Vanuatu Back Arc	worst case	7.96	200	30	6	40	170	0.9	3.3	0.4	2.6	2 h25'–3 h	2 h45'–3 h15'
Local source (rake 90°)														
15	Futuna Local	12 Mar 1993	7	40	15	2	60	300	0.1	4.9	0.1	3.6	0 h45'–1 h	0 h0–0 h15'

[1]: date of earthquake used as reference; [2]: magnitude used for the model, likely to differ from that of the reference earthquake; [3]: Fault Length; [4]: fault width; [5]: Length of slip along fault plane; [6]: Maximum Wave Elevation modelled above mean sea level; [7]: Maximum water height above ground; [8]: Estimated Time of Arrival of first wave/return to normal sea state; [9]: Estimate from Poprinet (2012) who uses a complex sub-fault model based on seismic inversion for this particular model; [10]: Not Detectable on model; [11]: Estimate from composite USGS model, see http://earthquake.usgs.gov/earthquakes/eqinthenews/2009/us2009mdbi/finite_fault.php.

the USGS (http://earthquake.usgs.gov) and NOAA databases (http://www.ngdc.noaa.gov). This is required to model the maximum credible magnitude for that fault.

Six scenarios (Sc. 1 to Sc. 6) were generated for trans-Pacific tsunamis, with sources located in Japan, the Kurils, the Aleutian-Alaska, Cascadia, Peru and Chile (Table 4).

For earthquake sources at offshore Japan (Sc. 1), fault parameters are based on the 11 March 2011 Japan event. As detailed in Popinet (2012), the source model used for the 2011 Tohoku tsunami is a collection of 190 sub-faults as defined by Okada (1985), and obtained by seismic inversion (Shao et al., 2011). The average slip thus given in Table 4 is only a summary of this information.

For the Kurils-Kamchatka region (Sc. 2), the fault parameters are based on the 15 November 2006 $M_W = 8.3$ central Kurils earthquake, the epicentre of which was located on the continental slope and the 13 January 2007 $M_W = 8.1$ earthquake located in Kurils–Kamchatka Trench (Rabinovich et al., 2008) (Fig. 6). Both earthquakes caused trans-Pacific tsunamis that were recorded in Hawaii, the west coasts of the United States, Peru, Chile, and New Zealand. The 2007 event had a 400 km-long rupture, but the $M_W = 9$ 1952 earthquake in the same region, suggests that longer ruptures are possible. Hence, we speculated a possible 1000 km-long rupture, as a worst case scenario. According to empirical relationships, this model would result in an $M_W = 9.28$ earthquake with a slip of about 17 m.

Tsunamigenic earthquakes in the Aleutian-Alaska include events in 1957, 1964, and 1965 (Johnson et al., 1994). For the Aleutian Arc scenario (Sc. 3), fault parameters are based on the 9 March 1957 earthquake, for which Johnson et al. (1994) indicate an 850 km-long rupture with 10 m displacement resulting in an $M_W = 8.6$. For the Cascadia, we used parameters for a worst case scenario as no recent detailed study provides reliable fault parameters. We assume a 1050 km-long rupture generating a $M_W = 9.1$ and a 17.5 m slip. This is in general agreement with published data (Christensen and Beck, 1994; Johnson et al., 1996).

For northern South America, events such as the 1906 Peru and 1868 Columbia-Ecuador were investigated (Beck and Nishenko, 1990). We used information from the 13 August 1868 $M_W = 9$ earthquake off Peru, which led us to using a 900 km-long rupture for a 15 m slip for Scenario 5 (Sc. 5).

Chile has a rich history of large tsunamigenic earthquakes (e.g., 1960, 2010) (Kanamori, 1977). Scenario 6 uses the 22 May 1960 $M_W = 9.5$ Chile earthquake as a guide for selecting the fault parameters along the Chilean Trench. Many variations on the fault parameters have been published and discussed for this earthquakes (e.g., Barrientos and Ward, 1990; Heinrich et al., 1996). Here, we selected a 920 km-long rupture and a 32 m seafloor displacement based on Heinrich et al. (1996) and references therein.

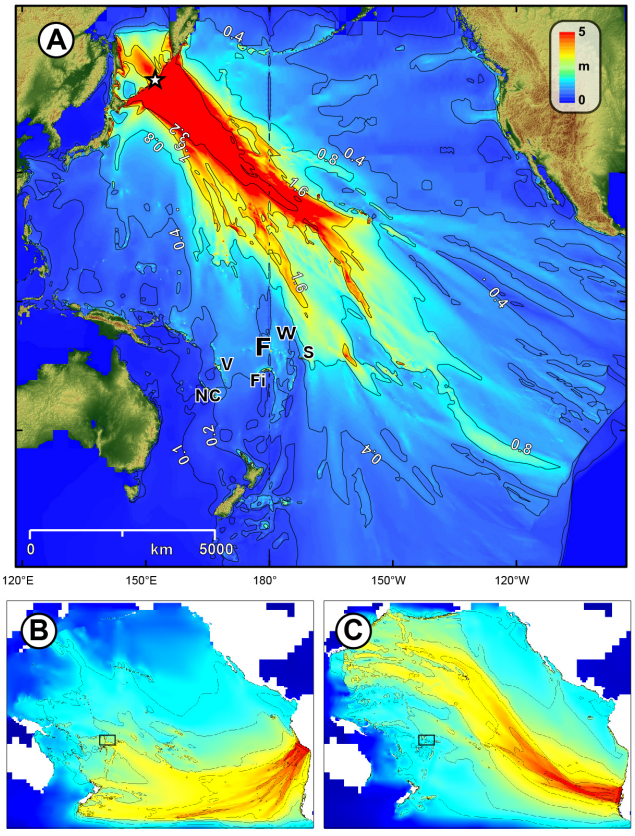

Figure 6. Tsunami maximum wave elevation (MWE in metres), across the Pacific Basin for **(a)** a $M_W = 9.1$ earthquake source along the Kuril Trench (Sc. 1, Table 4). Star indicates epicentre, F: Futuna, Fi: Fiji; NC: New Caledonia; S: Samoa; V: Vanuatu; W: Wallis; **(b)** a $M_W = 9$ Peru earthquake (Sc. 5) and **(c)** a $M_W = 9.29$ Chile earthquake (Sc. 6) Frame is approximate location of W&F. See Table 4 for source parameters. Models generated using the Gerris flow solver (Popinet, 2011).

5.2 Regional sources

Regional tsunamis are those with arrival times within 2 h of the triggering earthquakes. Regional earthquakes affecting W&F are associated with the Pacific-Australia plate boundary in the Southwest Pacific Region (Fig. 1). There are two seismically active regions likely to generate tsunamis of regional significance: The Tonga Trench and Vanuatu Arc to the SE and west of W&F respectively.

Other seismically active regions are unlikely to generate a tsunami. This is because the faults are either dominantly transcurrent or are small normal faults associated with rifting (Pelletier et al., 1998) and assumed to be of small magnitudes. Other tsunami generation mechanisms such as volcanic eruptions and landslides are not within the scope of this paper.

5.2.1 Tonga Trench

The Tonga Trench is the location of recurrent $> M_W = 8$ earthquakes. Two recent earthquakes have generated damaging tsunamis in the region on 26 June 1917 ($M_W = 8.4$) and 29 September 2009 ($M_W = 8.1$) (Engdahl and Villasenor, 2002; Okal et al., 2010). Both earthquake epicentres were ca. 110 km apart and about 550–650 km from Futuna and 400–500 km from Wallis.

Because of the significant, credible hazard that the Tonga Trench represents for the region in terms of earthquake-generated tsunamis, we ran five scenarios (Sc. 7 to 11) based on variations in sources parameters along the trench (Table 4; Fig. 5).

Scenario 7 is based on the 29 September 2009 rupture using parameters from Beavan et al. (2010) and Lay et al. (2010). These parameters were validated against post-tsunami observations made in Samoa (Dominey-Howes et al., 2009) and are further validated in this paper against our observation in Futuna-Alofi (Lamarche et al., 2010).

A full Tonga Trench scenario (Sc. 8) was generated using a 1000 km-long rupture resulting in a potential $M_W = 9.1$ earthquake with a 20 m slip. Such a length represents the entire Tonga segment of the Pacific-Australia plate boundary from its intersection with the Louisville Seamount Chain to the 90° turn of the plate boundary immediately south of Samoa (Fig. 5).

An extreme scenario (Sc. 9) was generated by adding an arbitrary 1 m water height at the time of the tsunami initiation for the previous case, i.e. a rupture of the entire Tonga Trench. It represents the impact of a tsunami arriving at the coast at high tide, consistent with the theoretical maximum tide amplitudes provided by the TPXO 7.2 global model of ocean tides of 1.55 m for Wallis and 1.65 m for Futuna (Egbert and Erofeeva, 2002, http://volkov.oce.orst.edu/tides/global.html).

A central Tonga scenario (Sc. 10) models a scenario along the central section of the Tonga Trench, similar to that of the September 2009 rupture, but with an increased fault length of 600 km.

A north Tonga scenario (Sc. 11) is based on a 300 km-long rupture along the NFTFZ, and a 6 m displacement generating an $M_W = 8.16$ event. This scenario models a rupture with an orientation likely to produce stronger effects on W&F.

5.2.2 Vanuatu

We tested three scenarios (Sc. 12 to Sc. 14) from the north Vanuatu, South Vanuatu and Vanuatu Back-Arc regions where a tsunami could be generated with impacts on W&F. These regions are located approximately 1400 km to the west of Futuna (Fig. 1).

The north Vanuatu fault source (Sc. 12) corresponds to the north Vanuatu Trench located west of the Vanuatu Archipelago. Based on the Vanuatu trench morphology, we used a 400 km-long rupture, oriented NNW–SSW, with 10 m displacement, resulting in an $M_W = 8.39$ event.

The south Vanuatu fault source (Sc. 13) runs in-line with the south Vanuatu Trench. It corresponds with the location of the 20 September 1920 $M_W = 8$ earthquake which generated a tsunami in the Loyalty Islands (Sahal et al., 2010). Based on the Vanuatu Trench morphology we used a 300 km-long rupture and 8 m displacement resulting in an $M_W = 8.24$ event.

The rupture parameters for the Vanuatu back-arc scenario (Sc. 14) are based on the 1999 $M_W = 7.5$ Ambrym earthquake (Régnier et al., 2003). This earthquake generated a tsunami in Vanuatu (Pelletier et al., 2000b). Using the tsunami numerical model of Ioualalen et al. (2006) for that event we used a fault length of 200 km capable of generating an $M_W = 7.96$ and a 6 m seafloor displacement along the central Vanuatu back-arc thrust zone (Table 4).

5.3 Local sources – Futuna-Alofi transform Fault

A local tsunami is an event for which the source is less than 100 km from the coast with arrival times of a few minutes. For this study, such sources are relevant to those along the Futuna-Alofi segment of the NFTFZ and resulting in a measurable hazard for Futuna only as it is too distant from Wallis (Figs. 2 and 5).

The scenario modelled here (Sc. 15) is based on the March 1993 $M_W = 6.3$ Futuna earthquake that produced a local tsunami in Léava (Louat et al., 1989a; Monzier et al., 1993). It is still unclear, however, as whether the tsunami was generated by the earthquake or indirectly by a submarine landslide that could have been triggered by the earthquake. Nonetheless, the tsunami was reported by local residents. We use the seafloor topography collected in October 1999, March 2000 and June 2011 (Pelletier et al., 2011, 2001, 2000a) to select a 40 km-long fault source with 2 m slip at the seafloor resulting in an $M_W = 7.0$ event.

6 Results

We only present a selected number of the 15 scenarios run in this study, which are most relevant for advancing our understanding of the tsunami hazard in W&F (Table 4). All scenarios are presented in Lamarche et al. (2013).

6.1 Pacific-wide sources

Out of the six Pacific-wide tsunamis scenarios, those showing the most significant impact on W&F are those from Japan, the Kurils and Peru. This is because of the regional topography of the Pacific Basin and the focusing of tsunami energy along particular pathways. Tsunamis originating from the Aleutians, Chile or Cascadia have minimal to no effect on our models, and are not discussed further in this paper (Fig. 6).

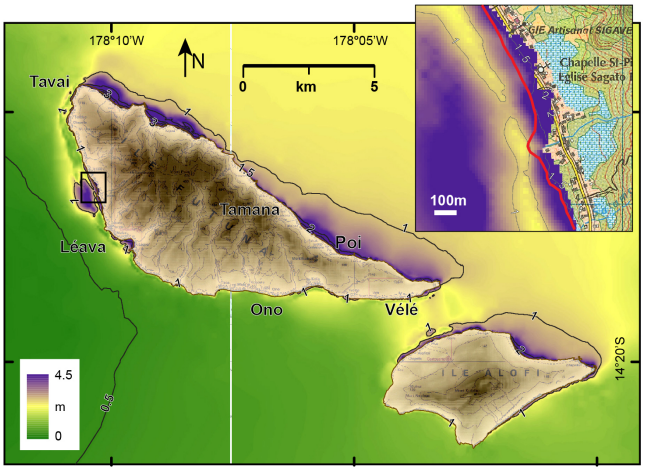

Figure 7. Maximum wave elevation at Futuna and Alofi modelled using the Gerris flow solver with an $M_w = 9.1$ earthquake source along the Kuril Trench (Fig. 5; Sc. 1, Table 4). Insert: zoom on amplification area on west coast of Futuna.

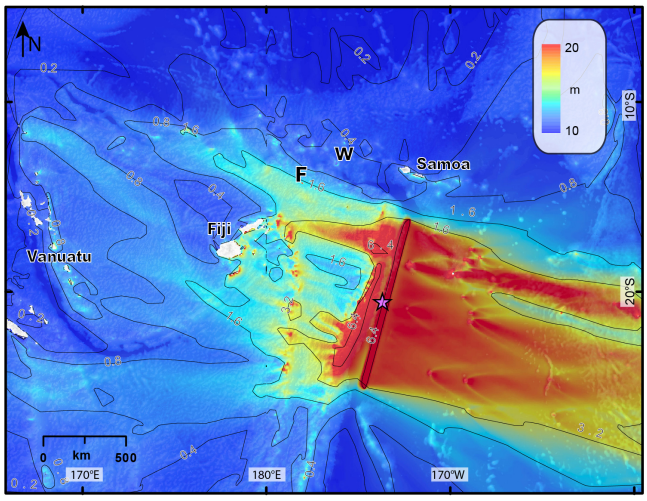

Figure 8. Tsunami maximum wave elevation (in m) generated by the full rupture of the Tonga Trench (Sc. 8, Table 4). Model generated using the Gerris flow solver. F: Futuna, W: Wallis. The star is the epicentre.

We note the strikingly different wave elevations resulting from the Peru (2.2 m in Wallis, 3.2 m in Futuna) and the Chile (0.7 m in Wallis, 0.5 m in Futuna) scenarios (Table 4). This counter-intuitive result is likely due to the focusing and defocussing effects within the deep Pacific Basin, which means that the Chile tsunami maximum wave train curves toward the northern Pacific region and misses W&F (Fig. 6b and c). We cannot rule out that the strike of the fault source plays a role in this particular result.

6.1.1 Wallis

ETA for tele-tsunamis range from 8 h30' for the Kurils to 15 h for Peru (Table 4).

MWEs do not exceed 70 cm anywhere inside the Wallis lagoon for the four tele-tsunamis modelled, and are never greater than 30 cm along the coast of the main island of Uvéa. Inundation distances or run-up are measurable in the models. MWEs are larger on the seaward wall of the barrier reef, with the largest MWE for the four scenarios being generated by the Kurils earthquake (Table 4) along the seaward shore of the south-eastern reef island of Faioa with an amplitude of 3.9 m. In the north, MWEs of 3.5 m are generated in the narrow passage between the islands of Nukufotu and Nukuloa, which suggests wave focusing, with the reef being potentially inundated. Generally the entire reef is inundated but the inundation depth does not exceed 1.5 m, except for these two cases.

6.1.2 Futuna and Alofi

ETA for tele-tsunamis in Futuna and Alofi ranges from 8 h50' for the Kurils to 15 h30' for Peru (Table 4).

All six tele-tsunamis modelled demonstrate that the areas most strongly impacted are the NE coast of Futuna and the NE and SE coasts of Alofi (Fig. 7), with MWEs of 4.5 m. MWEs of 2 m are modelled at the coast in the village of Pio, NE Futuna. Large MWEs are also generated along the coast on either sides of Chenal Vasia between Futuna and Alofi with MWE of ca. 1.5 m at Vélé and 2 m in Alofitai. The impact of tele-tsunamis is much weaker along the south coast of Futuna. To the west, a couple of areas show local amplification, in the Bay of Léava with MWE of 1 m and few kilometres northward with MWE of 1.5 m at the coast and run-up of 2.10 m at an inundation distance of not more than 100 m (Insert Fig. 7). Interestingly this inundation distance is the largest recorded for a trans-Pacific tsunami. In Tavai, at the NW tip of Futuna, the MWE reaches 3.4 m at the coast, with a run up of 4.45 m some 60 m from the coast.

Alofi is impacted by significant tsunami amplitudes from tele-tsunamis, with an MWE of 2.5 m in the NE. The beach in Alofitai is likely to be inundated with wave heights of 1.5 m at the coast impacting local shelters (falés). Inundation distances remain less than 50 m.

6.2 Regional source – Tonga Trench

The five scenarios using a source from the Tonga Trench (Table 4) generate tsunamis propagating eastward away from W&F (Fig. 8). A phenomenon also observed for the 2009 event (Beavan et al., 2010). The amplitude of the tsunamis varies considerably, with the largest event, which uses a 1000 km-long source, resulting in a MWE of 6.8 m in Wallis and 11 m in Futuna. We only provide a figure for the full Tonga Trench scenario.

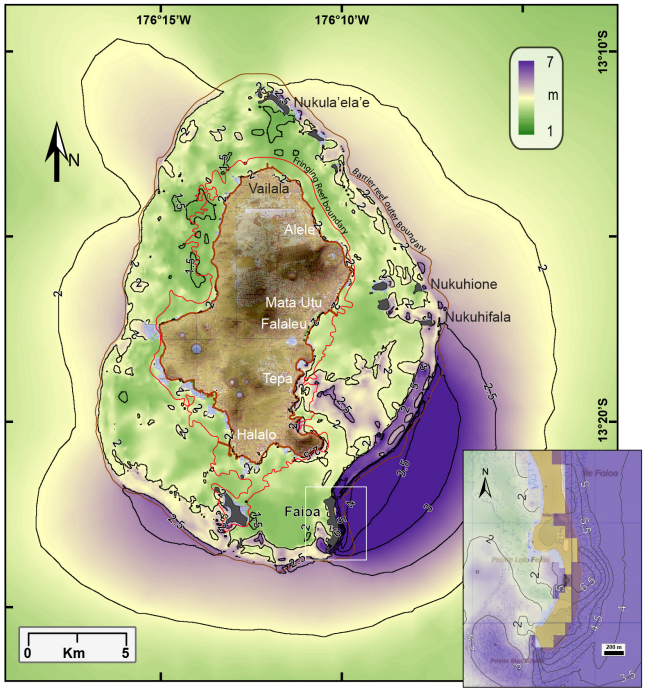

Figure 9. Maximum wave elevation (in m) at Wallis generated by an $M_W = 9.1$ earthquake along the Tonga Trench. Model generated using the Gerris flow solver. The outer boundary of the barrier reef (brown line) and the outer boundary of the fringing reef (red line) are from ReefBase database. Insert: enlargement on the reef island of Faioa.

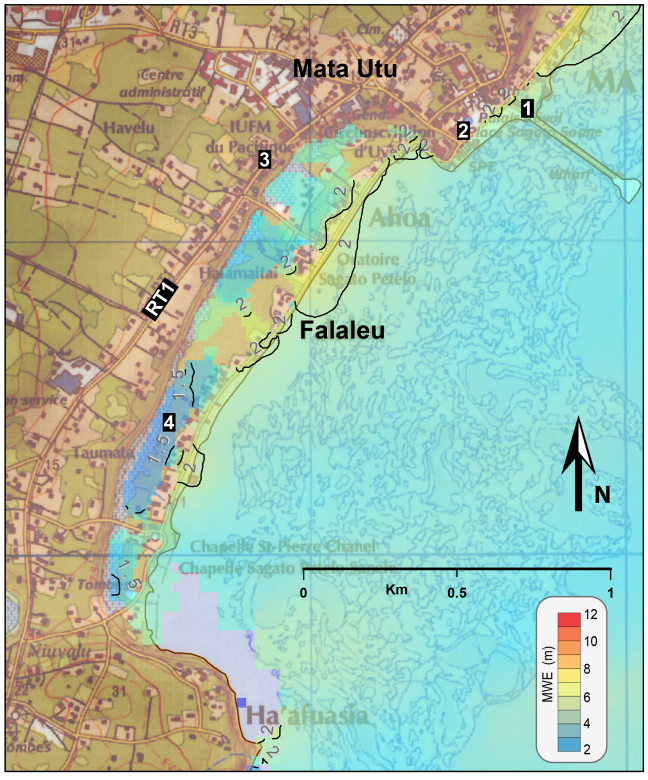

Figure 10. Maximum wave elevation and inundation map along the coast of central Uvéa (Wallis) from an $M_W = 9.1$ Tonga Earthquake (Sc. 8, Table 4). The 2 m MWE contour is drawn in places. Model generated using the Gerris flow solver. 1: port facilities; 2: Post Office and meeting place; 3: Teacher college; 4: Taro crops. RT1: Territorial Road N.1.

6.2.1 Wallis

ETA for the first wave ranges from less than 20 min to 1 h15, the shortest time corresponding to the scenario using the northern tip of the Tonga Trench source and the longest being for the full rupture of the Tonga Trench.

MWEs for all Tonga Trench scenarios range from 1.7 m for the central Tonga Trench source to 6.9 m for the full rupture +1 m. All Tonga scenarios look similar and we discuss the one resulting from the rupture of the full Tonga Trench (Fig. 9). Overall, the Wallis reef from the north (Nukufotu) clockwise to the SW (Passe Avatolu) experiences MWEs greater than 2 m.

The most affected area is along the SE, where most of the barrier reef around the island of Faioa is inundated with the largest MWEs modelled. Here the model predicts inundation distances greater than 100 m in the centre and northern part of the lagoon, which means that the tsunami would traverse Faioa Island in the southern half where it is at its lowest elevation thus forming an isthmus (Insert Fig. 9). South of Faioa, MWEs rise to 3 m above the reef. Nukuhifala and Nukuhione islands to the east of the barrier reef are also severely flooded with MWEs greater than 2 m on their east shores (seaward).

On Uvéa, inundation distances are greatest in Falaleu, Vailala, Gahi and Halalo (Fig. 9). In Falaleu, inundation distances reach 200 m corresponding to a run-up of less than 2 m (Fig. 10). Importantly, this results in flooding of taro fields behind the coastal dunes which are often lower than mean sea level. This represents a substantial hazard as taro is an important local food resource. In Mata'Utu, although the inundation distances do not exceed 80 m, the tsunami results in the flooding of the meeting place, the wharf and the administrative centre of the island as the MWEs at the coast range from 2 to 2.2 m. In Vailala, the inundation distance is greater than 300 m corresponding to a run-up of 2.4 m (Fig. 11), also resulting in the inundation of the taro fields inland from the coastal dunes. In the south, the inundation is severe in the Bay of Gahi, with MWE of 2.8 m at the coast and inundation distances greater than 150 m for run-ups higher than 2.5 m in the northern part of the bay (see discussion). Here too, the longest inundation distance does not necessarily correspond to the greatest run-up.

At Gahi, the run-up reaches 3.7 m at the shore although the inundation distances are no greater than 30 m as the shore abuts coastal cliffs (insert Fig. 16). This could also be a par-

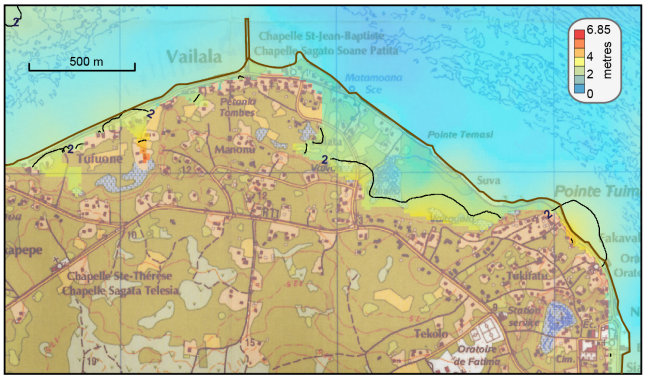

Figure 11. Maximum wave elevation and inundation map at Vailala along the northern coast of Uvéa (Wallis) from an $M_W = 9.1$ Tonga Earthquake. Model generated using the Gerris flow solver. The coastline from the IGN (2007) topo map is drawn in brown.

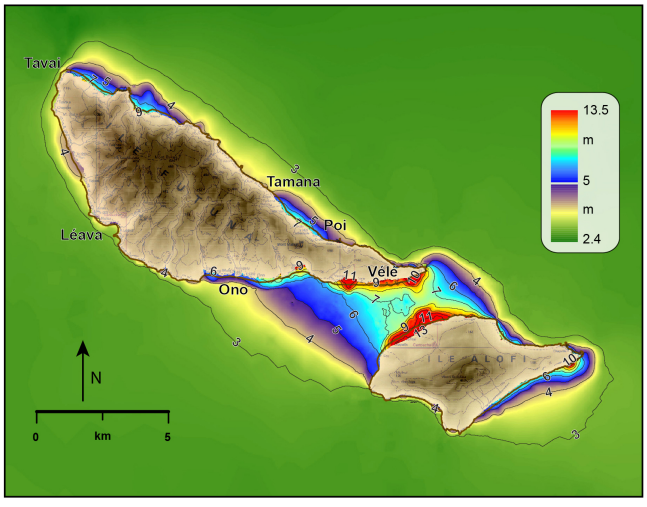

Figure 12. Maximum wave elevation (in m) at Futuna and Alofi generated by a $M_W = 9.1$ earthquake along the Tonga Trench.

ticular hazard as there is little to no place to take refuge between the cliff and shore. In Halalo, MWEs of 2.2 m are predicted at the coast with an inundation distance of up to 350 m, but the run-up does not exceed 2 m.

6.2.2 Futuna

ETA for the first wave ranges from less than 20 min to 1 h15 for tsunamis originating from the Tonga Trench. The predicted impacts are strongest along the shore of Chenal Vasia between Futuna and Alofi, along the south coast of Futuna, on the NE coast and around Poi (Fig. 12).

On the south coast, MWEs between 7 and 11 m are modelled between Vélé and Ono, with inundation distances reaching 130 m in Taoa and 200 m in Kolia (location on Fig. 4) with corresponding run-up elevations of 7 and 10 m, respectively.

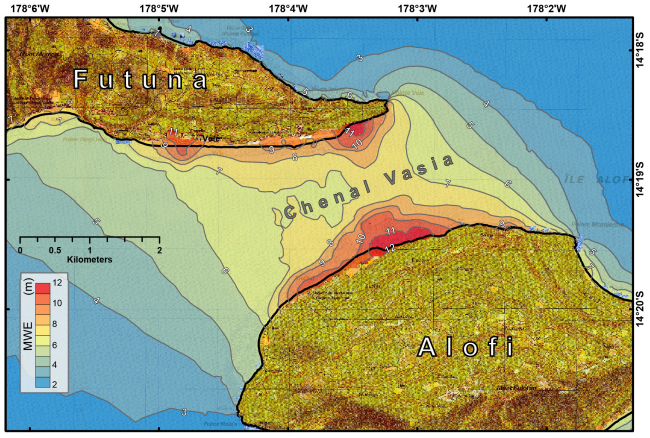

Figure 13. Maximum wave elevation (in m) and inundation map along the eastern tip of Futuna and NE Alofi from a $M_W = 9.1$ Tonga Earthquake. The coastline is highlighted by the bold line. MWE contours in m.

In the NE, MWEs may reach 7 m in Tavai and Tuatafa, with an inundation distance in the order of 120 m, and a run-up of 4 m. In Tuatafa, the September 2009 tsunami penetrated 45 m inland (Lamarche et al., 2010).

In Poi and Laloua, to the ENE of Futuna, MWEs are about 6 to 7 m, with inundation distances of approximately 80 m. This results in flooding of the road as was clearly observed during the 2009 tsunami (Lamarche et al., 2010). The small peninsula in Laloua is likely to be inundated at some stage.

More importantly and most noticeable is the amplification of the tsunami in Chenal Vasia between Alofi and Futuna, with the largest inundation distance of ca. 280 m modelled at Vélé, with a run-up of ca. 12.4 m (Fig. 13). Our model shows that the runway on the SE tip of Futuna would be completely flooded with inundation depth potentially as high as 5 m above the ca. 5 m high runway.

In Léava, amplifications during the few historical tsunamis match predictions, with an MWE of 1 m in the Bay of Léava. The modelled inundation distance in Léava is no more than 50 m. It is important to stress, as for all scenarios, that there is poor control on the bathymetry in the Bay of Léava and the model outputs therefore carry a reasonable uncertainty. This is especially true for the potential impact on the wharf.

The fringing reef around Futuna would be significantly inundated repetitively during an event such as a full rupture along the Tonga Trench. Witnesses reported three consecutive waves during the September 2009 tsunami, with the second one perceived as being the strongest (Lamarche et al., 2010). Assuming that the fringing reef is at sea level, the inundation depth is equal to the MWE, and our models predict potential values at the outer edge of the fringing reef of 9 m in Vélé, 3 m in Léava, 6 m in Tavai and Poi and 9 m in Alofitai.

Alofi is subject to significant tsunami amplitudes from this modelled event, with an MWE of 2.5 m in eastern Alofi

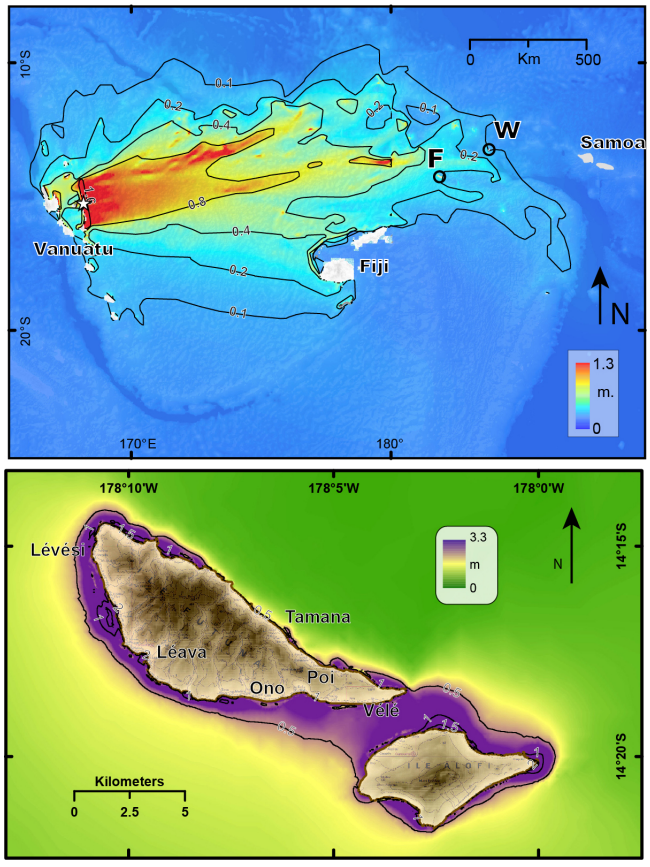

Figure 14. Maximum wave elevation (in m) from the source (top) and at Futuna (bottom) from a tsunami generated along the Vanuatu Back Arc (Sc. 14, Table 4). Star on top image is epicentre.

(Fig. 13). The beach in Alofitai is likely to be inundated with MWE of 1.5 m at the coast, with severe effects on the falés.

6.3 Regional Vanuatu back-arc source

The model, based on the $M_W = 7.5$ 1999 Ambrym earthquake (Régnier et al., 2003), generated a tsunami which propagated ENE directly toward W&F (Fig. 14). There is, however, no noticeable effect on Wallis for this scenario.

In Futuna and Alofi, the ETA is 2h45. The largest MWE of 3.3 m is predicted in the Bay of Léava, but the entire south coast is affected by MWE greater than 1 m. A wraparound of the tsunami wave is clearly visible around the NW of Futuna and all around Alofi (Fig. 14). The model shows small inundation distances, rarely greater than 30 m, as in Léava where a 2 m MWE is predicted. North of Léava, we modelled a MWE of 1.7 m at the coast with a penetration inland of 120–150 m arriving 2 h30' after the onset of the tsunami in Vanuatu. This scenario shows that coastal roads and buildings would be inundated north of Léava.

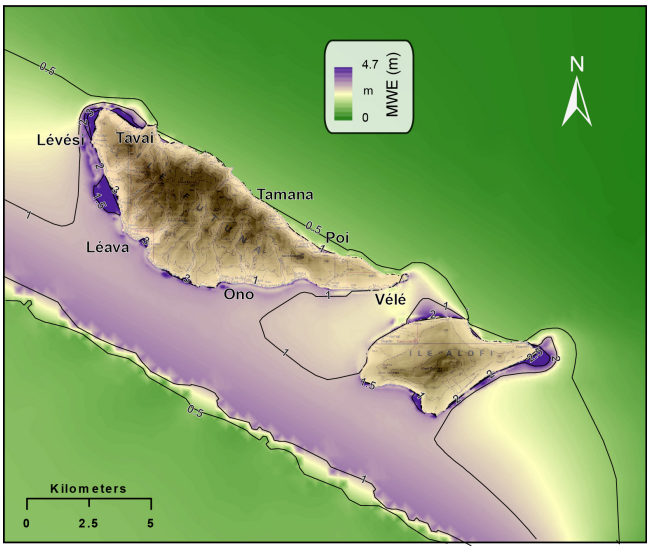

Figure 15. Maximum wave elevation (in m) at Futuna and Alofi generated from a local $M_W = 7$ earthquake along the Futuna Transform Fault (Sc. 15, Table 4, Fig. 2).

6.4 Local source

This scenario, based on the March 1993 $M_W = 6.5$ Futuna earthquake (Monzier et al., 1993), suggests a maximum tsunami height of 4.9 m hitting Futuna within minutes of its onset (Fig. 15). Wallis is not affected. The most noticeable effects are along the NW tip of Futuna where MWE reaches 4.9 m in the vicinity of Lévési, with a maximum inundation distance of approximately 80 m and in the Bay of Léava, where MWEs reach 3.7 m at the coast with inundation distances not exceeding 50 m.

The NE coast of Futuna is protected from this event, although a wrap-around effect is visible on the NW tip of the island which results in 3 m-high waves at the coast in Tavai. The SE coast is little affected even if the reef is inundated with a predicted MWE of ca. 1 m.

In Alofi, the most significant MWE is observed at the SE tip, i.e. opposite to the tsunami direction of arrival with MWEs greater than 2.5 m.

7 Discussion

7.1 Expected time of arrival

Procedures to calculate arrival times for trans-Pacific tsunamis are well established. Since Wallis and Futuna are ca. 260 km apart, tsunami ETAs differ. This is important when considering warnings and alarms. The time difference is 30 min for an event travelling east-west (Chile or Peru) and 40 min for events travelling from west to east (e.g., Vanuatu) (Table 4). Although the difference is small compared to the

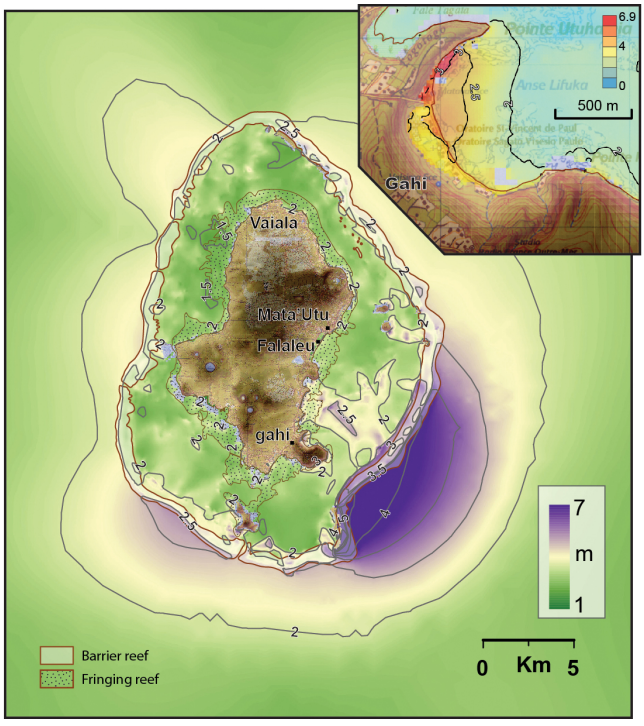

Figure 16. Synthesis of all maximum wave elevation models (in m) at Wallis for the 15 scenarios generated for this study. Insert: inundation map in Gahi, SE Uvéa.

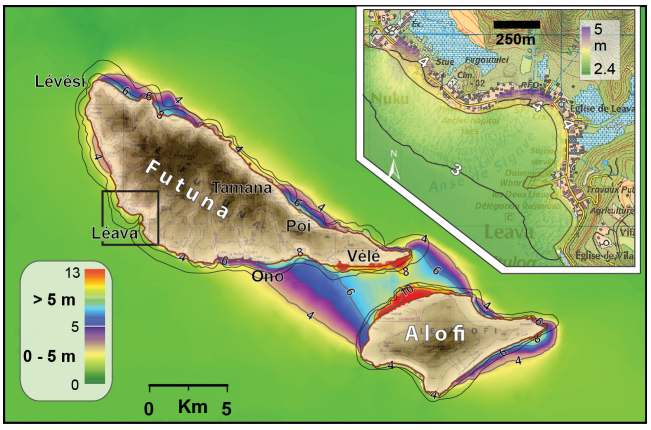

Figure 17. Synthesis of all maximum wave elevation models (in m) at Futuna and Alofi for the 15 scenarios generated for this study. Insert: focus on the Bay of Léava showing tsunami amplification on the administrative centre.

15 h of travel time for an event originating from sources such as Peru, it can be consequential for the onset of the alarm.

The return to normal will occur more rapidly further from the source, i.e. our model shows that a return to normal will occur in 17 h30 in Wallis and 15 h40 in Futuna for an event originating in Peru (Table 4). This counter-intuitive result is due to the lasting resonance occurring within the Wallis Lagoon. The resonance in the lagoon is a slow inner-reef effect, which is observed in the scenarios time-slices (or mpg movies – not shown here).

The time difference is indeed more problematic for local and regional events. For an event along the Futuna Fracture Zone, the tsunami ETA is less than 15 min for Futuna and 45 min for Wallis. In this case, the immediate corollary is that a tsunami warning cannot be delivered in time in Futuna from an overseas source. Although, our modelled event has no predicted impact on Wallis, a larger tsunami would require a rapid response in order to raise an alert in Wallis. Such a warning would most logically be delivered from Futuna, as a local earthquake would be felt strongly, as in 1840 and 1993.

An earthquake originating from the Tonga Trench may not be felt strongly enough in Wallis or in Futuna to raise an alert. An event originating from the northern tip of the Tonga Trench could generate a tsunami that would take only 10 min to reach Wallis (Table 4). In such a case, there may be little awareness of an impending tsunami. One of the most reliable signs may be an unusually rapid and large retreat of the sea at the shore. Educating coastal community about such signs is therefore essential (see e.g., http://www.ioc-tsunami.org).

Since the time required to process a scenario on a standard single-processor desktop computer is on the same order of magnitude to the physical time, it is conceivable to envisage using our method for real-time scenario modelling, to provide prediction and warning. This would, however, require optimisation of the Gerris codes to work on parallel processing, which is developed using the Basilisk free software program for the solution of partial differential equations on adaptive Cartesian meshes (http://basilisk.fr/).

7.2 Synthesis models

We generated compilations of the MWE for the 15 scenarios run in this study for Wallis (Fig. 16) and for Futuna and Alofi (Fig. 17). These are not scenarios per se, but provide information of the overall tsunami hazard by displaying the maximum wave elevation possible from all the scenarios tested. These models also provide the means to discuss the possible mitigating effects of the reef and lagoon on the tsunami (see next section).

These compilations match closely the models generated for the rupture of the full Tonga Trench (Figs. 9 and 12), the largest potential regional tsunami source from earthquake displacement for W&F. For Wallis, the highest hazard resides along the islands located on the barrier reef to the SE with MWE as high as 6.8 m on the outer reef. Two areas to the north (Vailala – Fig. 11), and the SSE coast have MWE locally as high as 2.5 m. Inside the lagoon, the highest MWE are modelled along the central-eastern side of Uvéa, with MWE as high as 2.5 m. Inside the rest of the lagoon MWE do not get higher than 2 m.

Figure 18. The fringing reef in Futuna (top) and the barrier reef in Wallis (Bottom).

In Futuna, as for Wallis, the synthesis of all scenarios matches almost exactly that of the Tonga Trench. Surprisingly, the effect of an event from the Futuna Fracture Zone has little significant impact on the overall hazard, although MWE as high as 4.9 m are predicted along the SW side of Futuna. The inundation distances are rarely greater than 50 m around the island, except to the east where distances as long as 130 m are observed at river mouths.

7.3 Mitigating effect of reefs and lagoons

W&F offer a variety of reef and lagoon morphologies. Whereas, in Wallis both fringing and barrier reefs surround Uvéa (Fig. 3), in Futuna there is only a narrow fringing reef (Fig. 4). The presence of narrow channels (passes) in the reef and the 30 m-deep lagoon in Wallis as well as the Léava embayment and the channel separating Futuna from Alofi (Chenal Vasia), provide geomorphic features that have distinct impacts on the development of a tsunami in terms of heights and inundation distances.

Although, we do not have quantitative information on the roughness of the reefs, our observations during field surveys strongly suggests that the reef in Wallis has a substantially rougher surface than in Futuna (Fig. 18). In Wallis the reef is covered with angular rocks of varying size, with most being 10–100 cm in diameter. The reef is also scattered with metre-scale pools which depths range from a few centimetres to a few metres, contributing to enhancing the surface roughness. In Futuna, the reef is more homogeneous than in Wallis, certainly smoother, and pools are shallower. Both reefs are scattered with boulders with sizes reaching up to a few metres in diameter (Fig. 18). While these observations need to be improved by measurements, they provide first order qualitative and relative information on the reef roughness.

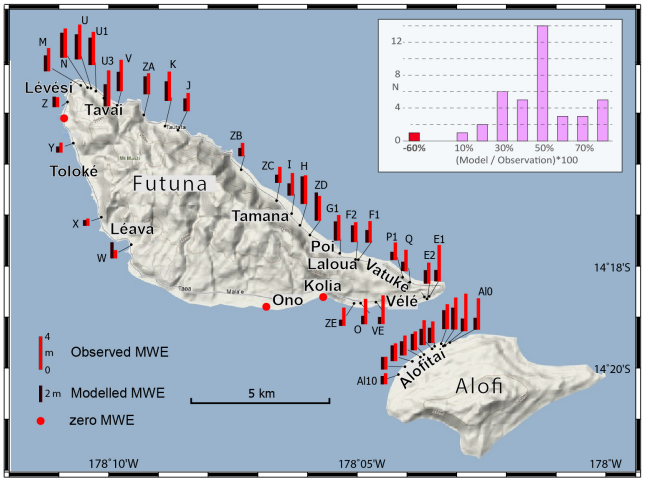

Figure 19. Observed (red) and modelled (black) maximum wave elevations (MWE) at Futuna and Alofi from the 2009 South Pacific Tsunami (Observed values from Lamarche et al., 2010). Modelled MWEs generated using the Gerris Flow solver. Insert: Modelled/observed MWEs expressed in percent.

Overall in Wallis the barrier reef dampens the tsunami amplitude, and attenuates its impact on the coast of Uvéa. This is demonstrated by the significantly lower MWEs inside the reef compared with that outside. For instance, the Tonga worst-case scenario generated a 6.9 m wave in SE Wallis and the highest waves at the coast of Uvéa is just under 3 m.

Whilst still a serious hazard to town and crops, this is substantially mitigated by the reef.

To the east, where the fringing reef connects with the barrier reef, the dampening effect seems to be less effective. Off Utulévé, (Fig. 3) the MWE is ca. 2.3 m both inside and outside the reef, suggesting that the continuity of the barrier reef with the fringing reef has a lesser effect on tsunami dampening. We speculate that this is a case that supports the inference of Gelfenbaum et al. (2011) that reefs a few hundred metres wide provide a balancing effect between tsunami amplification and dampening. We have no quantitative data for the roughness of the reef in this area.

The cuts in the barrier reef do not generate any amplification inside the lagoon, as has been described in other reef-surrounded islands such as in the Caribbean (Baba et al., 2008) or along Australia's Great Barrier Reef (Roger et al., 2012). We surmise that the passes are simply too narrow to produce this phenomenon.

Over the deepest part of Wallis lagoon, in the SE, there is a narrow SE–NW elongated area with MWE reaching 2.5 m. This zone of higher MWEs corresponds to the deepest part of the lagoon, and suggests resonance and amplification effects of the tsunami, with a resulting higher tsunami height at the coast (2.8 m high, Fig. 16). Inundation distance however, does not exceed 50 m. No unambiguous conclusions can be reached on the effect of the lagoon at this stage, and whether the lagoon provides some protection for Uvéa needs to be assessed in more detail with particular emphasis on the issue of amplification by resonance.

In Futuna, the largest MWEs occur on the coastline of Chanel Vasia between Futuna and Alofi. This suggests wave energy focusing is occurring between the islands. The fringing reefs are $\sim$ 550 and 280 m wide and provide little protection from the tsunami.

The NE tip of Futuna, around Tavai, also displays significant inundation heights compared to the rest of the island. This area is where we found evidence of palaeotsunamis from both geological markers and oral tradition (Lamarche et al., 2010). The reef in Tavai is only 100–120 m wide.

In Léava, amplification is predicted and it has been observed during historical tsunamis, with a MWE of 1 m in the Bay. The modelled inundation distance in Léava is no more than 50 m (Insert Fig. 17). There is, however, no good bathymetry for the bay and the model output therefore carries a reasonable uncertainty. This is especially true for the potential impact on the wharf. The reef all around Futuna will very likely be inundated repeatedly during such an event. This is corroborated by the September 2009 tsunami during which witnesses commented on three consecutive waves with the second one perceived as being the largest (Lamarche et al., 2010).

7.4 Inundation distances

Inundation distances are not as reliably generated by the models as MWE, essentially because this is highly dependent on onland topography. Unlike in Wallis, we do not have high-resolution coastal topography for Futuna. In contrast, some real events in Futuna can be used to validate our models (Lamarche et al., 2010), but this is not the case in Wallis. Indeed, the first important limiting factor for inundation distances in Futuna is the rapidly rising topography. However, the short inundation distances, rarely exceeding 50 m, all around the island were surprising. This is particularly so in the Bay of Léava where the focusing effects of the bay and opening in the reef would seem to enhance the wave, but we find no evidence of inundation reaching the road, let alone entering the taro field on the NE side of the village. Whilst this may be reassuring for the community, the poor quality of the bathymetry in the Bay increases our uncertainty about this particularly vulnerable area of the island.

Both observations and models clearly indicate that the longest inundation distances for the 2009 tsunami were along the shore of Chenal Vasia. Observations are 95 and 85 m in Futuna and Alofi respectively, compared with the model's predicted distances of 150 and 240 m. Indeed, it is not surprising that the predicted values are substantially larger, as the maximum extent of tsunami is known to be beyond the maximum extent of macroscopic tsunami deposits (Goto et al., 2011). Furthermore, the physical evidence for maximum tsunami inundation is transient and discontinuous geographically. Considering that Lamarche et al. (2010) survey happened 15 days after the event, some evidence may have already been removed by natural or human processes.

7.5 Models vs. observation

Comparing the models generated in this study with observations of the impact of the 2009 tsunami in Futuna and Alofi (Lamarche et al., 2010 and Fig. 16) enables us to discuss the limitations of using observations when assessing maximum inundation distances and MWEs. Here, we compare the 40 measurements of MWEs made after the 2009 tsunami with modelled values generated using the Tonga 2009 source (Fig. 19).

There is general correlation between observed and modelled MWEs in Futuna and Alofi, whereby both methods depict high tsunami impacts on NW Futuna and the NE coast, amplification of the tsunami in Chenal Vasia between Futuna and Alofi, and the mostly sheltered south coast (Fig. 19).

However, the modelled MWEs are on average 42 % lower than the observations (median 43 %), i.e. for an averaged observed wave elevation of 2.7 m the modelled value is 1.25 m. The agreement is better in NW Futuna and along the NE coast, with observations being on average 38 % higher than modelled MWEs.

The discrepancy between observed and modelled MWEs is exacerbated along the shore of Chenal Vasia where most observations are 60 % higher than that generated by our model, with differences reaching 80 % in Alofi. Even though amplification of the tsunami is predicted by the model in Chenal Vasia, the tsunami impact is likely to be stronger during future events.

The only observation which is substantially lower than the modelled MWE is in Léava, where the 1 m observed MWE corresponds to 1.62 m in our model. In Léava however, the observations were essentially inferred from photos and videos taken during the event, and interviews undertaken approximately 10 days later. No direct observations were possible anymore as the area had been cleaned.

The Gerris flow solver models have been validated using DART buoys and GLOSS tide gauges which supports our choice of initial source parameters. Comparisons with observations of the 2011 Tohuku event (Popinet, 2012) also reinforces the validity of the model. Hence, we believe that the most negative contribution to the models is the poor quality of the topography of reef and coastal fringe available for Futuna.

However, since tsunami amplification is not a linear process, the amount of energy generated at the source would not impact linearly on the coast of Futuna. This is substantiated by the case of the full Tonga Trench where the Chenal Vasia amplification is well shown.

The modelled and observed MWE data correlate well in places with palaeotsunami information inferred from trenches (Lamarche et al., 2010). This is the case in NW Futuna where the high waves predicted by the models as well as the high impact observed in October 2010 matches both geological palaeotsunami record and oral tradition. Here, we have four independent methods (observation, model, geological and oral tradition) that all point to a high tsunami hazard.

7.6 Uncertainties

Validation of the Gerris flow solver against DART data for the 2009 South Pacific tsunami provides us with a good level of confidence for our models. We anticipate that substantial uncertainties in the resulting models arise from the fault source parameters and the seafloor topography. The uncertainty related to the earth rigidity (μ) could be substantial in the case of tsunami earthquakes. In such cases, tsunamis are often substantially higher than that derived from the earthquake magnitude, and this can be accounted for by using a low rigidity (hence a higher slip) (e.g., Satake and Tanioka, 1999). However, we have not quantified these uncertainties in this paper.

As noted above, a particular weakness is the accuracy of the input bathymetry data, and most particularly in the very near coastal zone, i.e. in water depths less than ca. 10 m. Such water depths are not easily covered and necessitate specific equipment, e.g. LIDAR, and are usually time-consuming and therefore expensive projects. Assessing the uncertainty associated with the topography is difficult unless models are run before and after acquisition of high-resolution data sets, which is not the case here. It is worth noting that, in addition to the bathymetric resolution, the grid cell size used for modelling is an important source of uncertainty. A detailed bathymetry used in a poorly developed model may produce a poor fit.

Likewise, the topography of the coastal fringe, i.e. that portion of the coast that is likely to be inundated (say less than 10 m above mean sea level) is most often lacking accuracy for the Pacific Island. The issue is of dramatic importance for low lying islands such as a number of Pacific atolls (Orpin et al., 2015) where the highest elevation is often more than 5 m above mean sea level. The elevation data we acquired for the coastal fringe in Wallis enabled us to calibrate the DTM and strengthen our models. This was not done in Futuna, but there the topography with a narrow coastal fringe abuts steep cliffs makes it easier to devise escape routes. Ideally the very shallow (intertidal to 10 m depth) bathymetry should be acquired using a specific technique such as LIDAR. Once acquired the coastal topography and lagoon bathymetry should be merged into a single data set.

Assessing the uncertainty associated with the likelihood of occurrence of the tsunamis would require to develop probability of occurrence of the generating earthquakes, which is beyond the scope of this paper. However, based upon a growing database of palaeotsunami work throughout the Pacific region in areas such as Japan (Goto et al., 2014), Chile (Cisternas et al., 2005) and the SW Pacific (Goff et al., 2011), it would seem reasonable to suggest that the worst case scenarios discussed here are events that may occur about every 500–1000 years.

8 Conclusions

This paper presents 15 numerical models of tsunamis based on scenarios developed using the Gerris hydrodynamic software (Popinet, 2011) for modelling tsunami initiation, propagation and inundation. We used the best bathymetric and topographic information available for Futuna, whereas for Wallis we were able to acquire land elevation data using GPS RTK technology and derived the lagoon depth from satellite imagery. The tsunami sources were circum-Pacific fault sources which parameters were drawn from the published literature and are considered to be worst-case scenarios.

The results are the first numerical models of tsunami generation and inundation run for W&F and provide an overall assessment of the potential impact of tsunami for these isolated islands. The work demonstrates that the hazard associated with tsunami is significant for W&F.

The coastal areas that are most susceptible to inundation from Pacific-wide, regional and local earthquake-generated

tsunami are located on the SE coast of Wallis and the northern and eastern tips of Futuna.

The main island of Uvéa in Wallis is generally protected from hazardous tsunami by both barrier and fringing reefs. Modelling demonstrates that wave inundation heights of 2–3 m could occur on the populated SE coast of Uvéa, but the most significant hazard for Wallis occurs on the barrier reef.

The tsunami hazard on Futuna is significant. For several of the modelled scenarios the inundation depths in populated areas exceeds 2 m. As the majority of the domestic dwellings and infrastructure are in close proximity to the coast and, in most cases, are less than 2 m above sea level, such events could have a very serious impact.

Much of the W&F population live a few metres above sea level. It is therefore critical that, despite the possibly substantial uncertainties in the modelled scenarios, tsunami hazard information as these generated in this study is conveyed to the population of W&F. Better models will primarily come from improvement in the fault source parameters and in the quality of the seafloor topography in the coastal zone. It seems also relevant that the results of studies like this one should be incorporated into a proper risk assessment, including event probability of occurrence, cost of likely event, disaster response and land use planning. This study provides the material to develop such approaches.

The Supplement related to this article is available online at doi:10.5194/nhess-15-1763-2015-supplement.

Author contributions. G. Lamarche instigated and led the research project with B. Pelletier and J. Goff; S. Popinet and S. Delaux undertook the numerical modelling using the Gerris flow solver; G. Lamarche, B. Pelletier and J. Goff underook the Futuna survey in 2009. J. Goff led the palaeotsunami investigations. B. Pelletier, J. Mountjoy, J. Goff and J. Bind participated in the field trips in Wallis. J. Bind designed and ran the GPS survey in Wallis and derived the shallow Wallis lagoon water depths. G. Lamarche prepared the manuscript with contributions from all authors. J. Bind prepared the supplementary data part.

Acknowledgements. This work has benefited from financial support from the Pacific Fund of the French Ministry of Foreign Affairs, and the European Development funds channelled through SPC/SOPAC. Mr Enelio Liaufau from the *Direction de l'Environnement* in Wallis and Futuna was extremely supportive of our projects and provided excellent assistance during field investigations. *L'Administration Supérieure des îles Wallis et Futuna* supported our project and facilitated the funding from SPC-SOPAC. Land owners in both Wallis and Futuna were understanding of the needs of our research and enabled us to access their land for trenching. The bathymetric data around Wallis and Futuna acquired during the 1999 and 2000 cruises and WALFUT survey in 2011 were provided by IRD. Two anonymous reviewers and Guest Editor Hélène Hébert are thanked for their very constructive comments and suggestions for improvements on the manuscript.

Edited by: H. Hebert
Reviewed by: two anonymous referees

References

Andréfouët, S. and Diberg, G.: Cartographie et inventaire du système récifal de Wallis, Futuna et Alofi par imagerie satellitaire Landsat 7 ETM+ et orthophotographiquies aériennes à haute résolution spatiale, IRD, Nouméa, New Caledonia, 55 pp., 2006.

Aswani, S. and Graves, M. W.: The Tongan Maritime Expansion: A Case in the Evolutionary Ecology of Social Complexity, Asian Perspect., 37, 135–164, 1998.

Baba, T., Mleczko, R., Burbidge, D., Cummins, P., and Thio, H.: The Effect of the Great Barrier Reef on the Propagation of the 2007 Solomon Islands Tsunami Recorded in Northeastern Australia, PAGEOPH, 165, 2003–2018, 2008.

Barrientos, S. E. and Ward, S. N.: The 1960 Chile earthquake: inversion for slip distribution from surface deformation, Geophys. J. Int., 103, 589–598, 1990.

Beavan, J., Wang, X., Holden, C., Wilson, K., Power, W., Prasetya, G., Bevis, M., and Kautoke, R.: Near-simultaneous great earthquakes at Tongan megathrust and outer rise in September 2009, Nature, 466, 959–963, 2010.

Beck, S. L. and Nishenko, S. P.: Variations in the mode of great earthquake rupture along the Central Peru Subduction Zone, Geophys. Res. Lett., 17, 1969–1972, 1990.

Burley, D. V., Sheppard, P. J., and Simonin, M.: Tongan and Samoan volcanic glass: pXRF analysis and implications for constructs of ancestral Polynesian society, J. Archaeol. Sci., 38, 2625–2632, 2011.

Capecchi, B.: Les Conséquences de l'instabilité tectonique à Wallis et Futuna [consequences of tectonic instability in Wallis and Futuna], Cahiers d'Outre-Mer, 48, 381–400, 1995.

Chagué-Goff, C. and Goff, J.: Geochemical and sedimentological signature of catastrophic saltwater inundations (tsunami), New Zealand, Quaternary Australasia, 17, 38–48, 1999.

Chagué-Goff, C., Goff, J., Nichol, S. L., Dudley, W., Zawadzki, A., Bennett, J. W., Mooney, S. D., Fierro, D., Heijnis, H., Dominey-Howes, D., and Courtney, C.: Multi-proxy evidence for trans-Pacific tsunamis in the Hawai'ian Islands, Mar. Geol., 299–302, 77–89, 2012.

Christensen, D. H. and Beck, S. L.: The rupture process and tectonic implications ot the great 1964 Prince-William-Soun earthquake, PAGEOPH, 142, 29–53, 1994.

Cisternas, M., Atwater, B. F., Torrejón, F., Sawai, Y., Machuca, G., Lagos, M., Eipert, A., Youlton, C., Salgado, I., Kamataki, T., Shishikura, M., Rajendran, C. P., Malik, J. K., Rizal, Y., and Husni, M.: Predecessors to the giant 1960 Chile earthquake, Nature, 437, 404–407, 2005.

DeMets, C., Gordon, R. G., and Argus, D. F.: Geologically current plate motions, Geophys. J. Int., 181, 1–80, 2010.

Di Piazza, A. and Frimigacci, D.: A thousand years of gardening: a history of subsistence on Futuna, Bull. Indo-Pac. Prehist. Assoc., 11, 124–140, 1991.

Dominey-Howes, D. and Goff, J.: Tsunami Risk Management in Pacific Island Countries and Territories (PICTs): Some Issues, Challenges and Ways Forward, PAGEOPH, 170, 1397–1413, 2013.

Dominey-Howes, D., Thaman, R., and Goff, J.: UNESCO-IOC International Tsunami Survey Team Samoa (ITST Samoa), Interim Report of Field Survey 14th–21st October 2009, University of New South Wales, Sydney 2052, NSW, Australia, 190 pp., 2009.

Egbert, G. D. and Erofeeva, S. Y.: Efficient inverse modeling of barotropic ocean tides, J. Atmos. Oceanic Technol., 19, 183–204, 2002.

Engdahl, E. R. and Villasenor, A.: Global Seismicity: 1900–1999, Int. Handbook Earthq. Eng. Seismol., 81A, 665–690, 2002.

Frimigacci, D.: La préhistoire d'Uvéa (Wallis). Chronologie et periodization, Journal de la Société des océanistes, 111, 135–163, 2000.

Frimigacci, D., Keletaona, M., Moyse-Faurie, C., and Vienne, B.: La tortue au dos moussue – Ko le fonu tu'a limulimua, Texte de tradition orale de Futuna, Peeters Press, Paris, 1995.

Gelfenbaum, G., Apotsos, A., Stevens, A. W., and Jaffe, B.: Effects of fringing reefs on tsunami inundation: American Samoa, Earth Sci.-Rev., 107, 12–22, 2011.

Goff, J.: Evidence of a previously unrecorded local tsunami, 13 April 2010, Cook Islands: implications for Pacific Island countries, Nat. Hazards Earth Syst. Sci., 11, 1371–1379, doi:10.5194/nhess-11-1371-2011, 2011.

Goff, J., Chague-Goff, C., and Nichol, S.: Palaeotsunami Deposits: A New Zealand Perspective, Sediment. Geol., 143, 1–6, 2001.

Goff, J. R., Chague-Goff, C., Etienne, S., Lamarche, G., Pelletier, B., Richmond, B. M., Strotz, L. C., Buckley, M. L., Wilson, K., Dudley, W. C., Urban, G., Sale, M., and Dominey-Howes, D.: Identifying Precursors to the 2009 South Pacific tsunami?, San Francisco, 2009.

Goff, J., Lamarche, G., Pelletier, B., Chagué-Goff, C., and Strotz, L.: Predecessors to the 2009 South Pacific tsunami in the Wallis and Futuna archipelago, Earth Sci.-Rev., 107, 91–106, 2010a.

Goff, J., Nichol, S. L., Chagué-Goff, C., Horrocks, M., McFadgen, B. G., and Cisternas, M.: Predecessor to New Zealand's largest historic trans-South Pacific tsunami of 1868 AD, Mar. Geol., 275, 155–165, 2010b.

Goff, J., Chagué-Goff, C., Dominey-Howes, D., McAdoo, B., Cronin, S., Bonté-Grapetin, M., Nichol, S., Horrocks, M., Cisternas, M., Lamarche, G., Pelletier, B., Jaffe, B., and Dudley, W.: Palaeotsunamis in the Pacific Islands, Earth Sci.-Rev., 107, 141–146, 2011.

Goff, J., Chagué-Goff, C., Nichol, S., Jaffe, B., and Dominey-Howes, D.: Progress in palaeotsunami research, Sediment. Geol., 243–244, 70–88, 2012a.

Goff, J., McFadgen, B. G., Chagué-Goff, C., and Nichol, S. L.: Palaeotsunamis and their influence on Polynesian settlement, The Holocene, 22, 1061–1063, 2012b.

Goto, K., Chagué-Goff, C., Fujino, S., Goff, J., Jaffe, B., Nishimura, Y., Richmond, B., Sugawara, D., Szczuciński, W., Tappin, D. R., Witter, R. C., and Yulianto, E.: New insights of tsunami hazard from the 2011 Tohoku-oki event, Mar. Geol., 290, 46–50, 2011.

Goto, K., Ikehara, K , Goff, J., Chague-Goff, C. and Jaffe, B.: The 2011 Tohoku-oki tsunami – three years on, Mar. Geol., 358, 2–11, 2014.

Hanks, T. C. and Kanamori, H.: A moment magnitude scale, J. Geophys. Res., 84, 2348–2350, 1979.

Hébert, H., Schindelé, F., and Heinrich, P.: Tsunami risk assessment in the Marquesas Islands (French Polynesia) through numerical modeling of generic far-field events, Nat. Hazards Earth Syst. Sci., 1, 233–242, doi:10.5194/nhess-1-233-2001, 2001.

Heinrich, P., Guibourg, S., and Roche, R.: Numerical modeling of the 1960 Chilean tsunami, Impact on French Polynesia, Phys. Chem. Earth, 21, 19–25, 1996.

IGN: Futuna Alofi, Carte de Randonnée 1:25,000. N.4902, Institut Géographique National, Paris, 2007a.

IGN: Wallis, Carte de Randonnée 1:25,000. N.4901, Institut Géographique National, Paris, 2007b.

Ioualalen, M., Pelletier, B., Watts, P., and Regnier, M.: Numerical modeling of the 26th November 1999 Vanuatu tsunami, J. Geophys. Res., 111, C06030, doi:10.1029/2005JC003249, 2006.

Johnson, J. M., Tanioka, Y., Ruff, L. J., Sataki, K., Kanamori, H., and Sykes, L. R.: The 1957 great Aleutian earthquake, PAGEOPH, 142, 3–28, 1994.

Johnson, J. M., Satake, K., Holdahl, S. R., and Sauber, J.: The 1964 Prince William Sound earthquake: Joint inversion of tsunami and geodetic data, J. Geophys. Res-Solid Earth, 101, 523–532, 1996.

Kanamori, H.: Mechanism of Tsunami Earthquakes, Phys. Earth. Panet. Inter., 6, 246–259, 1972.

Kanamori, H.: The energy release of great earthquakes, J. Geophys. Res., 82, 2981–2987, 1977.

Lamarche, G., Pelletier, B., and Goff, J. R.: Historique des tsunamis sur l'Archipel de Futuna: Fréquence, magnitude et impact sur la communauté insulaire, Rapport de Mission 6–17 Octobre 2009, [Historical tsunami in the Futuna Archipelago: Frequency, magnitude and impact on the community], NIWA Client Report, Wellington: Fonds de Coopération Economique, Sociale et Culturelle pour le Pacifique du Ministère des Affaires Etrangères et Européenne [Pacific Funds of the French Ministry of Foreign and European Affairs], pp. 15., NIWA, Wellington, Unpublished field trip report, 2009.

Lamarche, G., Pelletier, B., and Goff, J.: Impact of the 29 September 2009 South Pacific Tsunami on Wallis and Futuna, Mar. Geol., 271, 297–302, doi:10.1016/j.margeo.2010.02.012, 2010.

Lamarche, G., Mountjoy, J., Popinet, S., Pelletier, B., Goff, J. R., Bind, J., and Woelz, S.: L'aléa tsunami à Wallis et Futuna Modélisation numérique et inventaire des tsunamis [Tsunami Hazard in Wallis and Futuna. Scenario-based numerical modelling and paleo-tsunami record], Administration supérieure du Territoire de Wallis et Futuna, Wallis Island, Wellington, NZ, 86 pp., 2013.

Lay, T., Ammon, C. J., Kanamori, H., Rivera, L., Koper, K. D., and Hutko, A. R.: The 2009 Samoa-Tonga great earthquake triggered doublet, Nature, 466, 964–968, 2010.

Louat, R., Frohlich, C., Charvis, P., Hello, Y., McPherson, P., Nakamura, Y., and Pontoise, B.: Etude d'un essaim de séismes dans le sud de Vanuatu (SO Pacifique) par un réseau de stations sismologiques sous-marines (OBS), Comptes Rendus Acad. Sc., 2, Paris, 309, 213–218, 1989a.

Louat, R., Monzier, M., Grzesczyk, A., Dupont, J., Eissen, J. P., and Maillet, P.: Sismicité superficielle à proximité des iles de Horn (Territoire de Wallis et Futuna-Pacifique Sud): caractéristiques et conséquences [Shallow seismicity near the Horn Islands (Territory of Wallis and Futuna – South Pacific): origins and hazards], Comptes Rendus Acad. Sc., 2, Paris, 308, 489–494, 1989b.

Løvholt, F., Glimsdal, S., Harbitz, C. B., Zamora, N., Nadim, F., Peduzzi, P., Dao, H., and Smebye, H.: Tsunami hazard and exposure on the global scale, Earth-Sci. Rev., 110, 58–73, 2012.

Monzier, M., Régnier, M., and Decourt, R.: Rapport sur la crise sismique de mars 1993 à Futuna (TOM des îles Wallis et Futuna), rapport de missions, centre Orstom de Nouméa, 30, 1993.

Mountjoy, J. J., Pelletier, B., Lamarche, G., Goff, J. R., Pilarczyk, J. E., and Bind, J.: Les Grands Tsunamis Historiques et Paléo-Historiques a Uvéa (Wallis et Futuna): Fréquence, Magnitude et Impact sur les Communautés Insulaires. Rapport de mission 29 Aout–10 Septembre 2011 [Large Historic and Paleo-Historic Tsunami on Uvéa (Wallis et Futuna): Origin, Timing and Associated Hazard and Risk. Field trip report 29 August–10 September 2011]. NIWA Client Report. NIWA, Wellington: Fonds de Coopération Economique, Sociale et Culturelle pour le Pacifique, pp. 19., 2011.

NGDC: National Geophysical Data Center (NGDC) (2014) Global Historical Tsunami Database. Boulder, CO, NGDC, available at: http://www.ngdc.noaa.gov/hazard/tsu_db.shtml, last access: September 2014.

Okada, Y.: Surface deformation due to shear and tensile faults in a half-space, Bull. Seismol. Soc. Am., 75, 1135–1154 1985.

Okal, E. A.: Seismic parameters controlling far-field tsunami amplitudes: A review, Nat. Hazards, 1, 67–96, 1988.

Okal, E. A., Borrero, J. C., and Synolakis, C. E.: Evaluation of Tsunami Risk from Regional Earthquakes at Pisco, Peru, Bull. Seismol. Soc. Am., 96, 1634–1648, 2006.

Okal, E. A., Fritz, H. M., Synolakis, C. E., Borrero, J. C., Weiss, R., Lynett, P. J., Titov, V. V., Foteinis, S., Jaffe, B. E., Liu, P. L. F., and Chan, I. C.: Field Survey of the Samoa Tsunami of 29 September 2009, Seismol. Res. Lett., 81, 577–591, 2010.

Orpin, A., Rickard, G., and Gerring, P.: Tsunami hazard potential for the equatorial southeastern Pacific atolls of Tokelau from scenario-based simulations, Nat. Hazards Earth Syst. Sci. Discuss., in press, 2015.

Pelletier, B. and Louat, R.: Seismotectonics and present-day relative plate motions in the Tonga-Lau and Kermadec-Havre region, Tectonophysics, 165, 237–250, 1989.

Pelletier, B., Calmant, S., and Pillet, R.: Current tectonics of the Tonga–New Hebrides region, Earth Planet. Sci. Lett., 164, 263–276, 1998.

Pelletier, B., Lagabrielle, Y., Benoit, M., Cabioch, G., Calmant, S., Garel, E., and Guivel, C.: Newly identified segments of the Pacific-Australia plate boundary along the North Fiji transform zone, Earth Planet. Sci. Lett., 193, 347–358, 2001.

Pelletier, B., Lagabrielle, Y., Cabioch, G., Calmant, S., Régnier, M., and Perrier, J.: Transpression active le long de la frontiere décrochante Pacifique-Australie: Les apports de la cartographie multifaisceaux autour des iles Futuna et Alofi (Pacifique sud-ouest) [Active transpression along the fast Pacific-Australian transform boundary revealed by swath mapping around the Futuna-Alofi Islands], Comptes Rendus Acad. Sc., 2, Paris, 331, 127–132, 2000a.

Pelletier, B., Regnier, M., Calmant, S., Pillet, R., Cabioch, G., Lagabrielle, Y., Bore, J.-M., Caminade, J.-P., Cristopher, I., and Temakon, S.: Le séisme d'Ambrym-Pentecôte (Vanuatu) du 26 novembre 1999: données préliminaires sur la séismicité, le tsunami et les déplacements associés, Comptes Rendus Acad. Sc. , 2, Paris, 331, 21–28, 2000b.

Pelletier, B., Andréfouët, S., Liaufau, E., Mountjoy, J., and Panche, J.-Y.: Cartographie des pentes externes des récifs barrière de Wallis et Futuna, Campagne WALFUT du N.O. ALIS (13–19 juin 2011), Unpublished voyage report, IRD, Nouméa, New Caledonia, 15 pp., 2011.

Popinet, S.: Gerris: a tree-based adaptive solver for the incompressible Euler equations in complex geometries, J. Comput. Phys., 190, 572–600, 2003.

Popinet, S.: Quadtree-adaptive tsunami modelling, Ocean Dynam., 61, 1261–1285, 2011.

Popinet, S.: Adaptive modelling of long-distance wave propagation and fine-scale flooding during the Tohoku tsunami, Nat. Hazards Earth Syst. Sci., 12, 1213–1227, doi:10.5194/nhess-12-1213-2012, 2012.

Power, W., Downes, G., and Stirling, M.: Estimation of tsunami hazard in New Zealand due to South American earthquakes, PAGEOPH, 164, 547–564, 2007.

Rabinovich, A. B., Lobkovsky, L. I., Fine, I. V., Thomson, R. E., Ivelskaya, T. N., and Kulikov, E. A.: Near-source observations and modeling of the Kuril Islands tsunamis of 15 November 2006 and 13 January 2007, Adv. Geosci., 14, 105–116, doi:10.5194/adgeo-14-105-2008, 2008.

Régnier, M.: Sismotectonique de la ride de Horn (iles de Futuna et Alofi), un segment en compression dans la zone de fracture Nord-Fidjienne [Seismotectonics of the Horn ridge (Futuna and Alofi islands), a segment uplifted by compression in the Fiji fracture zone], Comptes Rendus Acad. Sc., 2, Paris, 318, 1219–1224, 1994.

Régnier, M., Calmant, S., Pelletier, B., Lagabrielle, Y., and Cabioch, G.: The Mw7.5 1999 Ambrym earthquake, Vanuatu: A back arc intraplate thrust event, Tectonics, 22, 1034, doi:10.1029/2002TC001422, 2003.

Roger, J., Dudon, B., Sédilot, B., Zahibo, N., and Pelinovsky, E.: Tsunami hazard mitigation by coral reef protection for the French Caribbean Islands, Lisbon, Portugal, 2012.

Sahal, A., Pelletier, B., Chatelier, J., Lavigne, F., and Schindelé, F.: Un catalogue des tsunamis en Nouvelle-Calédonie du 28 mars 1875 au 30 septembre 2009 [A catalog of tsunamis in New Caledonia from 28 March 1875 to 30 September 2009], Comptes Rendus Geoscience, 342, 434–447, 2010.

Satake, K. and Tanioka, Y.: Sources of Tsunami and Tsunamigenic Earthquakes in Subduction Zones, PAGEOPH, 154, 467–483, 1999.

Satake, K., Rabinovich, A., Dominey-Howes, D., and Borrero, J.: Introduction to "Historical and Recent Catastrophic Tsunamis in the World: Volume II. Tsunamis from 1755 to 2010", PAGEOPH, 170, 1361–1367, 2013.

Schindelé, F., Hébert, H., Reymond, D., and Sladen, A.: L'aléa tsunami en Polynésie française : synthèse des observations et des mesures, Comptes Rendus Acad. Sc., 2, Paris, 338, 1133–1140, 2006.

Shao, G., Li, X., Ji, C., and Maeda, T.: Focal mechanism and slip history of the 2011 Mw 9.1 off the Pacific coast of Tohoku Earthquake, constrained with teleseismic body and surface waves, Earth Planet. Space, 63, 559–564, 2011.

SHOM: Iles Wallis, 1:20,000. N.6876, 2nd Edn., Service hydrographique et océanographique de la marine, Brest, France, 2008.

SHOM: Iles Futuna et Alofi, 1:60,000. N.7234, 2nd Edn., Service hydrographique et océanographique de la marine (SHOM), Brest, France, 2010.

Sugawara, D., Goto, K., and Jaffe, B. E.: Numerical models of tsunami sediment transport – Current understanding and future directions, Mar. Geol., 352, 295-320, 2014.

Wells, D. L. and Coppersmith, K. J.: New empirical relationships among magnitude, rupture length, rupture width, rupture area, and surface displacement, Bull. Seismol. Soc. Am., 84, 974–1002, 1994.

Williams, S. P.: Tsunami Hazard, Samoan Islands: Palaeotsunami Investigation, Numerical Modelling and Risk Implications, 2014.PhD Thesis, University of Canterbury, Christchurch, New Zealand, 2014.